January 2018

Regolith Transport Rates And Grain Size Distributions On Hillslopes, Sierra Nevada, Ca

Timothy Wuenscher

REGOLITH TRANSPORT RATES AND GRAIN SIZE DISTRIBUTIONS ON HILLSLOPES, SIERRA NEVADA, CA

by

Timothy James Wuenscher
Bachelor of Science, Texas A&M University, 2016

A Thesis

Submitted to the Graduate Faculty

of the

University of North Dakota

in partial fulfillment of the requirements

for the degree of

Master of Science

Grand Forks, North Dakota

December
2018

This thesis, submitted by Timothy James Wuenscher in partial fulfillment of the requirements for the Degree of Master of Science from the University of North Dakota, has been read by the Faculty Advisory Committee under whom the work has been done and is hereby approved.

Dr. Jaakko Putkonen

Dr. William Gosnold

Dr. Taufique Mahmood

This thesis is being submitted by the appointed advisory committee as having met all of the requirements of the School of Graduate Studies at the University of North Dakota and is hereby approved.

Grant McGimpsey
Dean of the School of Graduate Studies

September 27, 2018

Date

PERMISSION

Title Regolith Transport Rates and Grain Size Distributions on Hillslopes, Sierra Nevada, CA

Department Harold Hamm School of Geology and Geological Engineering

Degree Master of Science

In presenting this thesis in partial fulfillment of the requirements for a graduate degree from the University of North Dakota, I agree that the library of this University shall make it freely available for inspection. I further agree that permission for extensive copying for scholarly purposes may be granted by the professor who supervised my thesis work, or in his absence by the Chairperson of the department or the dean of the School Graduate Studies. It is understood that any copying or publication or other use of this thesis or part thereof for financial gain shall not be allowed without my written permission. It is also understood that due recognition shall be given to me and to the University of North Dakota in any scholarly use which may be made of any material in my thesis.

Timothy James Wuenscher

9/11/2018

TABLE OF CONTENTS

LIST OF FIGURES

LIST OF TABLES

ACKNOWLEDGEMENTS

I would like to thank my research advisor (Dr. Jaakko Putkonen) and the other members of my advisory committee (Dr. Taufique Mahmood, Dr. William Gosnold) for their assistance and guidance throughout the completion of my Master's degree at the University of North Dakota.

I would also like to thank Dr. Risa Madoff and Liam Kolb for their assistance with the field work required to complete my research.

Thanks to the Abbott Ball Company for providing me with quality aluminum spheres on short notice.

Special thanks to my parents who have always supported me in my academic pursuits.

ABSTRACT

Earth's landforms constantly change as a result of erosion at the surface. Surface regolith is composed of a variety of different grains sizes, each having a different rate of transport. The varying rates of transport between grain sizes cause the distribution of grain sizes to change along hillslopes over time. The ability to predict grain size distributions as a function of time would be useful for determining slope stability and determining ages of landforms. However, current knowledge is limited for the varying rates of transport of different grain sizes. To better understand grain transport rates, a set of experiments was carried out in Mono Basin, CA, where glacial moraines provide ideal hillslopes to measure grain transport rates and grain size distributions. This data was used within a hillslope diffusion model to simulate transport of grains and generate grain size distributions along the slope over time.

Results from the field experiments showed that transport rate does not necessarily increase with decreasing grain size, and that there may be a certain grain size (1-4 mm) that has the highest velocity on hillslope surfaces. This may be due to cohesiveness of finer grains, a buoyancy of coarser grains in the mobile surface layer, a tendency of finer grains to experience intermittent burial, or a combination of all three factors.

The measured grain size transport rates are consistent with the transport rates predicted by the best fit of the grain size distribution model, which also suggested that

grains within the 1-4 mm grain size class have the highest downslope transport rate. The grain size distribution model can somewhat accurately predict grain size distributions at the footslope and crest of the moraines over time.

LIST OF ABBREVATIAIONS

AG – Aluminum grains (0.7 mm and 3 mm diameter grains)

MBO – Mono Basin moraine

MBY – Tahoe moraine

PB – Pebbles (30 mm)

SS – Sediment sample

CHAPTER I

INTRODUCTION

1.1 Background and motivation

The surface of the Earth is constantly changing due to erosion and transport of material to other locations. Erosion occurs as a result of natural environmental factors such as rainfall and wind, as well as anthropogenic processes associated with human developments. The field of geomorphology is centered on the transport of Earth's surface sediment (known as regolith) and the changes that result from this transport. The movement of regolith results in patterns of degradation on landscapes that can provide insights as to how certain landforms are created.

Natural erosion is generally aided by moving water (e.g., rain, rivers, etc.) and/or gravity (mountainous areas with steep slopes). Wind can also aid erosion if the regolith is made up of particles light enough to be carried. Knowing the rates at which regolith moves on hillslopes is necessary to make informed decisions about land and hazard management (National Research Council, 2000). Additionally, measuring rates of regolith transport on desert hillslopes has been used to determine the age of landforms (Hallet and Putkonen, 1994) and paleoclimates (Madoff, 2015), which can give information not only about desert regions but also help explain past climates worldwide.

Perhaps the first recorded interest in the subject of regolith transport at the Earth's surface came with Charles Darwin in the late 1800s, when he took a keen interest in the

way earthworms disrupted the upper layers of soil, tracking the way they circulated ash and lime spread on the surface (Darwin, 1881, as referenced by Freeman, 1977). Later on, scientists attempted to identify the primary mechanisms by which regolith is transported. Two such mechanisms have been widely discussed: landsliding and soil creep (Leopold et. al., 1966; Schumm, 1967; Selby, 1982; Saunders and Young, 1983; Abrahams et. al., 1984).

Landsliding involves a large volume of regolith moving downslope all at once, with landslide events being sporadic in time and space. Landsliding occurs as a result of events that cause instability in slopes, such as heavy precipitation, earthquakes, or a steep slope gradient. Regions with steep slopes and plentiful rainfall are much more prone to landslides than regions with low slopes and little rainfall.

Soil creep refers to any relatively slow and steady progression of the upper layer regolith downhill. Rates of soil creep are affected by several factors, including vegetation, precipitation, and steepness of slopes. Soil creep is a universal process; it occurs everywhere on Earth where there is loose, unconsolidated regolith at the surface. It is one of the key processes that guide mathematical models of landscape evolution (Oehm and Hallet, 2005).

Modeling the way landforms change is important because it can allow for predictions about the way Earth's surface evolves. Measurements of regolith transport, such as soil creep, can act as inputs to mathematical models. Surfaces that are steeply sloped will evolve more rapidly; soil creep and landslides are much more effective at steeper slopes because gravity overcomes friction more easily. Therefore, models are

especially useful for predicting the degradation rates of high-relief landscape features like hills and mountains.

W.M. Davis (1892) was one of the first to hypothesize that soil movement created convex hilltops. This idea was expanded upon years later when the first basic model for steep cliff decay was postulated (Lehman, 1933). In the 1960s it was discovered that equations used to model heat flow could also be used to model the diffusive effects of hillslope erosion (Culling, 1960, Scheidegger, 1961).

The hillslope diffusion equation has been used several times in the past to model the way that elevation along a slope changes over time (e.g., Carson and Kirkby, 1972; Hallet and Putkonen, 1994; Putkonen and Swanson, 2003; Putkonen and O'Neal, 2006; Putkonen et. al., 2012). This equation tells us how the general form of a hillslope changes; steep slopes will gradually become less steep over time, as regolith moves from areas with steep slopes and accumulates in areas with more gentle slopes. It is called hillslope diffusion for this reason; the surface material is spread out more widely over time, dissipating any unevenness.

The hillslope diffusion model can tell us about how the form of the hillslope changes over time, but does not give any direct insights as to how regolith actually moves across the surface. It simply says that over a certain amount of time, a certain volume of regolith will be transported from the crest of the hillslope to the foot of the hillslope. How can this volume of regolith be characterized; how does it move and what is its composition?

Regolith at the surface is not uniform in composition—that is, rarely will regolith be composed of sediment grains that are all exactly the same size. Grains of different

sizes will not move in the same way—for example, a pea-sized pebble will probably be transported down a hillslope more quickly than a car-sized boulder. Regolith is usually a mixture of many differently sized grains, all which have various rates of transport. Rates of transport of certain grain sizes have been investigated in many studies (e.g., (Schumm, 1964; Kirkby and Kirkby, 1974; McLaren and Bowles, 1985, Gabet, 2003; Shi et al., 2012). Because of differing transport rates between grain sizes, certain grain sizes may become more concentrated at certain places on a hillslope. The difference in this relative amount of grains present according to their size is referred to as the grain size distribution.

Knowledge of the distribution of regolith grain sizes, within a geologic context, is a useful method of describing geomorphic settings and the significance of surface dynamics in the natural environment. On local scales, grain size distribution can help to distinguish the regolith transport processes that lead to current surface conditions (Visher, 1969). In addition to its use as a tool for interpretation of surface processes, knowing the grain size distribution on a landform may offer insight into the stability of the surface (e.g., Van Burkalow, 1945; Zhou et. al., 2013). There are other implications for landform composition as well: the field of geoarchaeology examines particle size distributions of buried sites to determine conditions under which the sediments were deposited, which could also help determine age of deposits (Waters, 1997).

While understanding the origins of grain size distributions on hillslopes is important, it is poorly understood. On some scree slope surfaces, the average grain size increases downslope (Statham, 1973; Kirkby and Statham, 1977). On more weathered slopes with a smaller mean grain size, the opposite generally holds true. There must be a

reason for this difference in grain size distribution. If grain size distributions are the result of varying transport rates of different grain sizes, then knowing the rates at which different grains travel should provide understanding of how grain size distribution changes through time. However, little is known about how different grain sizes are transported across sloped surfaces. One reason this process is poorly understood is the lack of information available for transport rates of fine grains (<1 mm in diameter). Fine grains are present in large quantities in almost all environments around the Earth, and more are constantly being generated as a result of the weathering of larger grains. At the Sierra Nevada field site in this study, for example, 35% of the volume of surface regolith consists of grains smaller than 1 mm. Another reason transport rates for grain sizes are poorly understood is the lack of measurements of different grain sizes in the same area over the same time period. It is important to be able to directly compare transport rates between grain sizes, because the differences will explain the differentiation of the grains along the slope over time.

In this study, hillslopes at the base of the Sierra Nevada Mountains in California are examined to determine the way regolith is transported, and how this affects the grain size distribution over time. The Sierra Nevada experiences little rainfall, and can be classified as an arid landscape. The slope angles of the hillslopes are low enough (<30°) to be characterized as stable for granitic-rock hillslopes in dry desert regions (Melton, 1965). Because of this, it is unlikely that any landslide events occur on these hillslopes; regolith transport should only be the result of soil creep.

To summarize, the objectives of this study are as follows:

- Measure the transport rates of different grain sizes at the field site.

- Create a mathematical model that can accommodate different transport rates for different grain sizes. The output of this model should be a prediction of grain size distributions along the hillslope.
- Compare the output of the model to the grain size distributions seen in the field.

The desired result of this study is a model that can accurately determine the grain size distribution anywhere on the slope at any time through its history, in addition to monitoring the way the slope profile evolves.

The ability to predict grain size distributions along a slope over a period of time is very useful. Zhou and others (2013) tested many aggregates of different soil-rock compositions and found there to be a wide range of stabilities of certain aggregates depending on the grain size distribution and lithology of the source rock. Knowing beforehand how the grain size distribution will evolve could prevent land stability issues in construction on natural landscapes or engineering projects involving artificial slope construction. Additionally, if the model is able to predict grain size distribution at any point in time, presumably it should be possible to predict the grain size distribution of the subsurface to the depth at which regolith has accumulated. This would be useful for any projects that involve excavation of regolith, and the depth of certain grain size distributions could potentially help to determine the age of subsurface regolith. Finally, if we know what grain size distributions to expect on landforms at a given time, we may be able to determine the ages of entire landforms by matching what is seen in the modeled age to the observations in the field. At the very least, this may provide further evidence to support or refute previously calculated ages of landforms.

1.2 Study Area

The field area in this study is the Mono Basin region on the west side of the Sierra Nevada Mountains in eastern California. These mountains are known for being previously glaciated during glacial periods in recent geologic history, and these glaciers produced lateral moraines at their periphery. Lateral moraines are parallel ridges of debris produced when debris along the edges of alpine glaciers is left behind as glaciers retreat. This field work in this study was conducted on the flanks of two of these lateral moraines. These moraines selected for this study provide an ideal testing ground for this study due to their localized uniform slope angles and different ages.

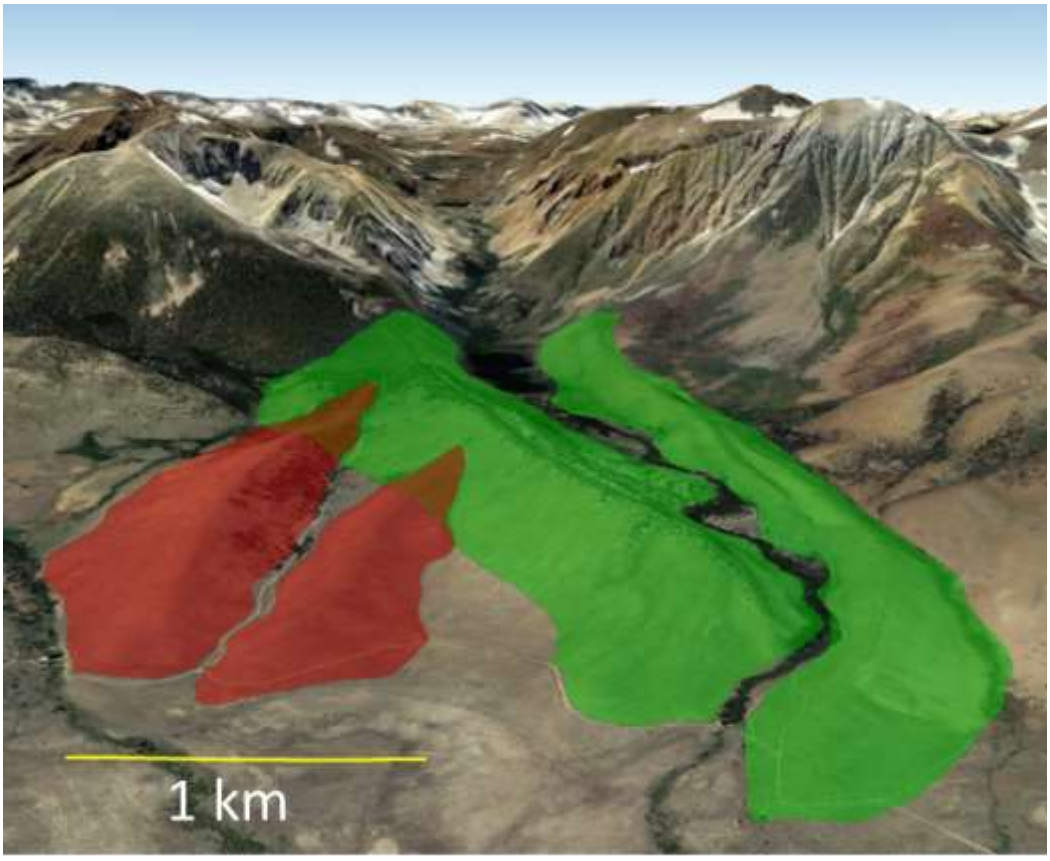

Figure 1.1. The Mono Basin and the nested Tioga, Tahoe, Sherwin, and McGee moraines. The Mono Basin Moraines (red, left) are approx. 100 kyr old. The set of four nested moraines (green, right) vary in age. The Tahoe moraines in this study are approximately 45 kyr old. The older, the Mono Basin moraines were cross-cut by the younger sets of moraines as the later glaciations flowed out of the valley and deposited material on top of them. Image generated using Google Earth.

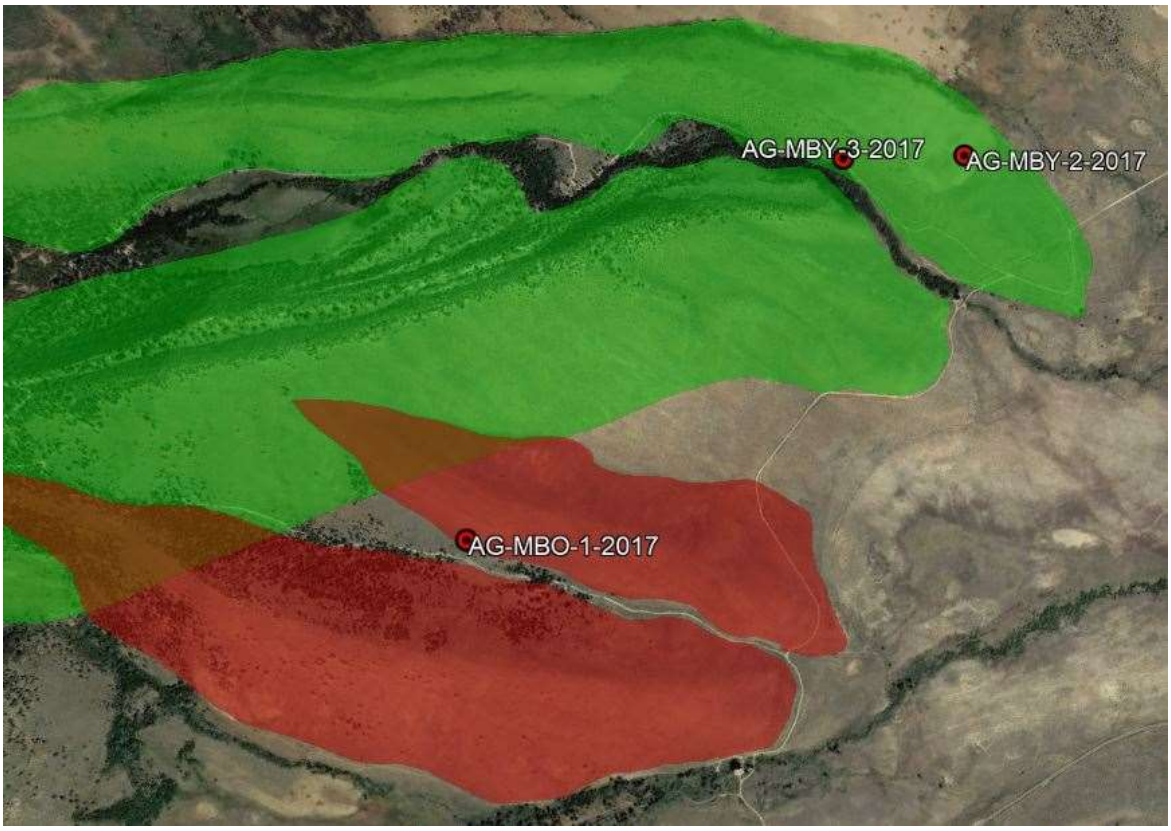

Fig 1.2. Locations of each study site on the moraines. Site MBO-1-2017 was on the southern side of the left-lateral Mono Basin moraine. Site MBY-3-2017 was on the southern side of the left-lateral Tahoe moraine. Site MBY-2-2017 was on the northern side of the northern Tahoe moraine. These three sites were selected for their differing local slope angles (14°, 20°, and 27°, respectively).

Data were collected on two moraines in this study: the left-lateral Mono Basin moraine and left-lateral Tahoe moraine (Fig. 1.1, Fig. 1.2) adjacent to Sawmill Canyon and Bloody Canyon, respectively. The coordinates of the field area are 37.881384° N, 119.138300° W. The Mono Basin moraines have been dated within the range of 80-120 kyr through cosmogenic exposure dating of surface boulders; the Tahoe Moraines have been dated at approximately 40-60 kyr using the same method (Phillips et al., 1990). However, there is considerable debate about the numeric ages of the moraines in the Sierra Nevada (Gillespie and Clark, 2011), especially the moraines that are believed to be

older. The Tahoe moraines accompany a larger set of moraines that are nested within each other; these include, from youngest to oldest, the Tenaya, Tioga, and Tahoe moraines, named after their respective glaciation events leading to them (Phillips, 1990; Gillespie and Clark, 2011). The moraines in this study have differing surface grain size distributions; generally, the Mono Basin moraines have a homogenous mixture of smaller grains while the Tahoe moraines are more heterogeneous and contain more pebbles and boulders. This may be due to the increased weathering of the older moraines resulting in a more thorough breakdown of grains (Sampson, 2006), and other factors relating to surface regolith transport that will be investigated in this study. The regolith in this area is a mixture of granitic sand (quartz, feldspar and clay minerals) and larger granitic pebbles and boulders.

CHAPTER II

METHODS

2.1 Distributing grains

To acquire sufficient data to determine relative surface velocities of different grain sizes, the surface velocities of three different grain sizes were measured. The three different grain diameters were: 0.7 mm, 3 mm, and 30 mm. These grain sizes were selected in order to best describe the main mobile constituents of hillslope material at this field site (see Table 3.7, 3.8 for exact measurements). About 50% of the measured volume of the moraines is comprised of grains between 0.7-30 mm in diameter. Grains smaller than 0.7 mm are too small to be individually tracked with current best known methods.

To measure surface velocity of these grain sizes, their transport distance must be measured over a period of time. One of the difficulties faced in this task is that grains must be somehow marked to identify them at a later time after they are transported. In a previous study by Kirkby and Kirkby (1974), native grains were painted white and later located. This has worked in the past at the field site in this study for 30 mm grains, but in a test setting was found to be quite unreliable for the 0.7 mm and 3 mm grains. It was difficult to locate the small painted grains after they were mixed in with other regolith as the grains quickly got dusty and lost their distinct painted color. Instead of tracking native 0.7 mm and mm grains, artificial aluminum grains were used as a substitute.

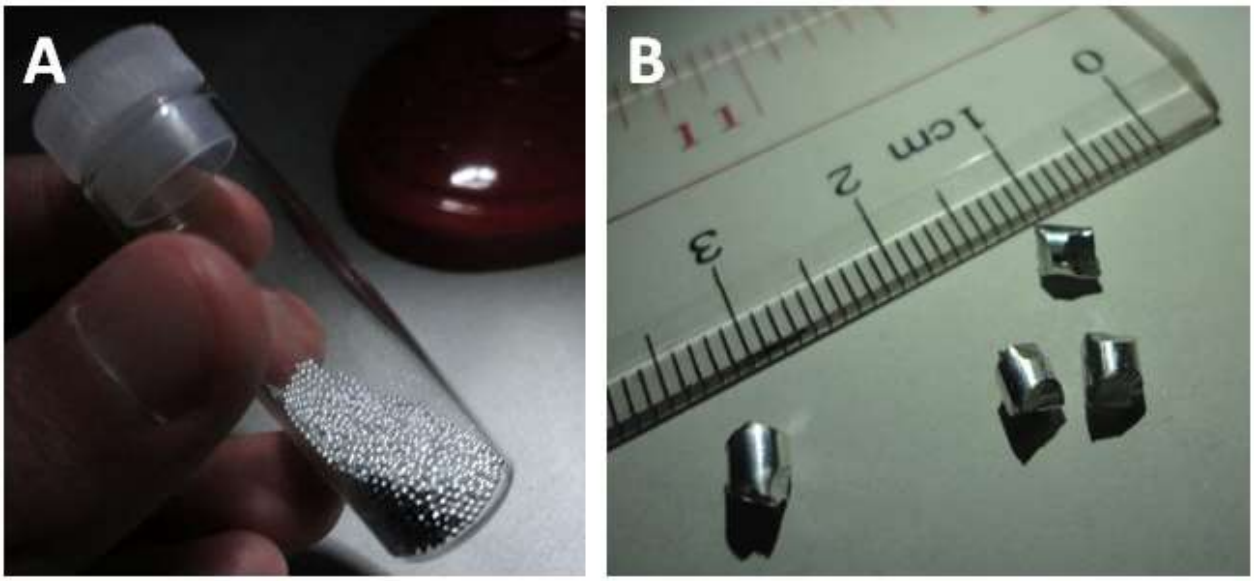

Figure 2.1. Aluminum grains. (A) 0.7 mm aluminum grains. (B) 3 mm aluminum grains

To simulate the fine grains, 0.7 mm diameter aluminum balls were used (Fig. 2.1) for the purpose of being able to later locate the grains upon sample collection, due to its reflectiveness. Generally speaking, the more spherical a particle is the easier it is to transport because only rolling friction needs to be overcome (Statham, 1977). The 0.7 mm particles are small enough to where the friction needed to be overcome is small regardless, but the particle sphericity is still important to keep in mind, as irregularly shaped particles would probably be more representative of the actual hillslope material. Aluminum was used because it has a similar density (2.7 g/cm^3) compared to the quartz-feldspar sand found in the field area (~2.6 g/cm^3). For the 3 mm grains, a 3 mm diameter aluminum rod was cut into segments that measured 3 mm in diameter along their shortest axis and between 3-5 mm on their longest axis. For the remainder of this study they will be referred to as 3 mm grains. (Fig 2.1). For the 30 mm grains, pebbles native to the field site were painted white and numbered to easily locate them. Grains were distributed on

May 17, 2017, and collected on August 26, 2017. The total duration of this experiment was 101 days.

0.7 mm and 3 mm grains

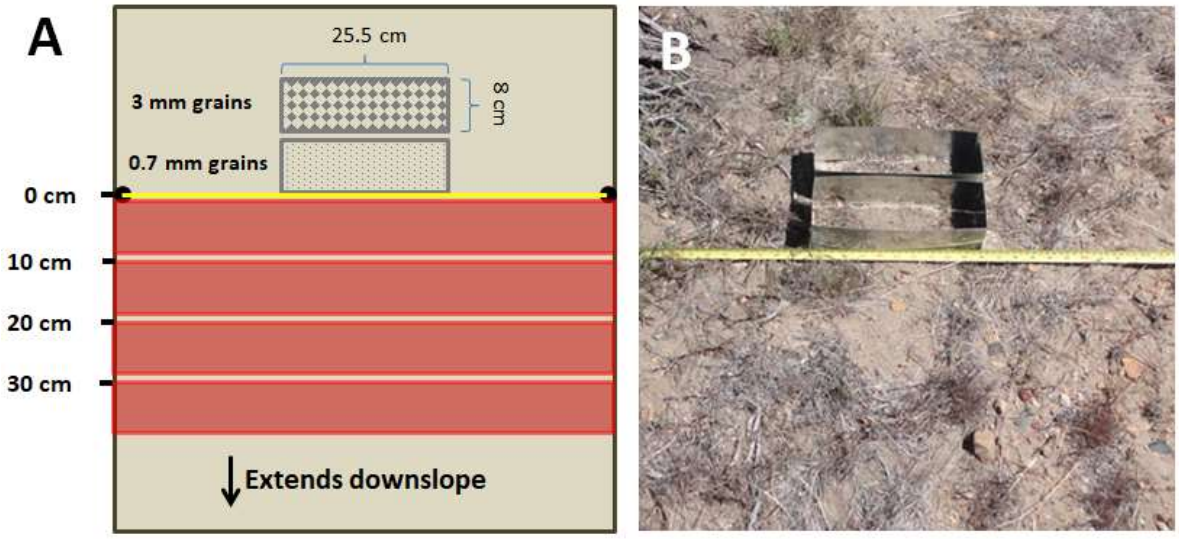

Figure 2.2. (A) Overhead view of setup of aluminum grain sites. Grey boxes are the areas of initial grain placements. Red boxes represent areas where samples were collected (8 cm in width, with 2 cm between each sample swath). Depending on the site, the sampling extended down the slope to as much as 2.5 m. (B). Actual image of site setup.

The 0.7 mm grains (3,000 per site) were evenly distributed into an area of hillslope (8 x 11) cm to a side using an open-bottomed metal box to contain the grains. The 3 mm grains (100 per site) were evenly distributed into the same area of hillslope immediately upslope of the 0.7 mm grains. After the grains were distributed inside the box, the box was remove from the hillslope. This is shown in Fig. 2.2. This setup was repeated for 3 sites, at 14 degree, 20 degree, and 27 degree slope angles at each site respectively. Performing this experiment at different slope angles was done to be able to directly compare the effects of slope angle on grain surface velocities.

30 mm pebbles

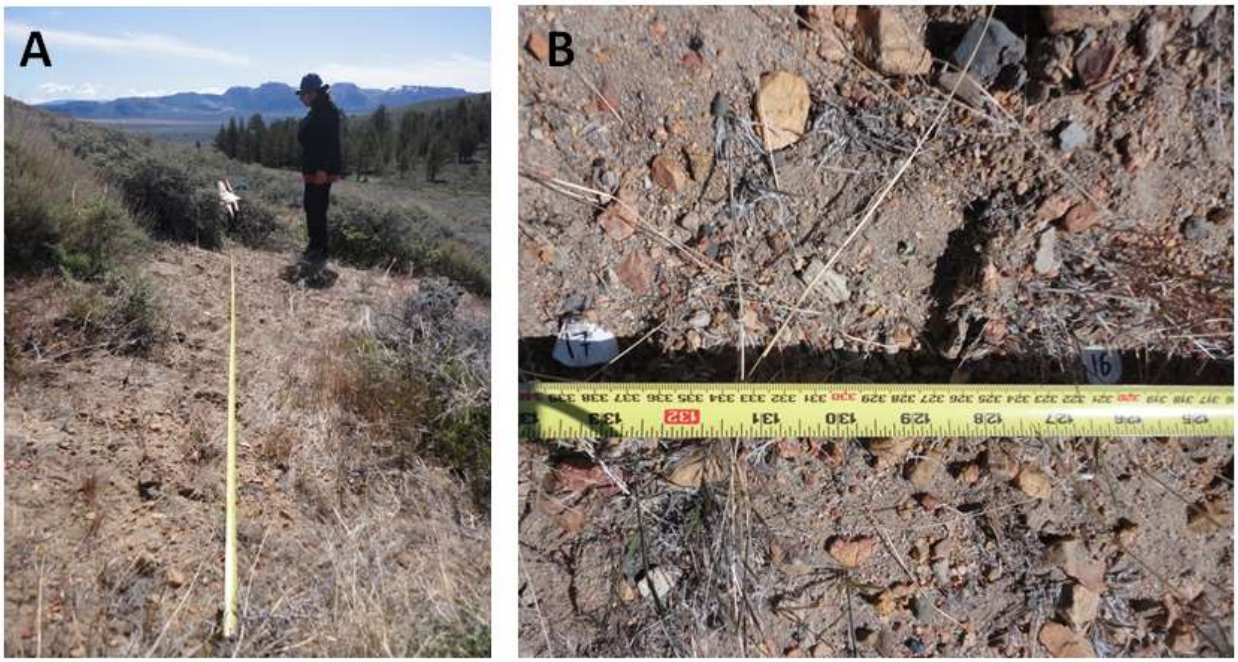

Figure 2.3. 30 mm pebble placement. (A) Pebbles were placed under span of long tape every 20 cm. (B) Two pebbles after being placed in their starting position.

30 mm pebbles were set in a line perpendicular to the slope of the hill, using a long tape and rebar to denote the exact placement of the pebbles. The pebbles were distributed along this line at 20 cm intervals along the tape measure. Each pebble was numbered using a permanent marker to ensure they did not get mixed up during future measurements. 3 of these pebble line sites were set up in close proximity to their corresponding aluminum grain sites, again at 14, 20 and 27 degree slope angles. This process is shown in Fig 2.3.

2.2 Collection of grains

0.7 and 3 mm grains

The 0.7 mm and 3 mm grains were collected downslope from their initial positions on the hillslope. Surface regolith samples were taken using the metal boxes (8 x 25.5 cm) in swaths at regular intervals (see Figure 2.2), using a small scoop to take samples approximately 5 cm deep within each swath to ensure all grains that moved downslope were collected, even if they were slightly buried. The regolith for each swatch was bagged for later processing to recover the individual grains. The 2 cm gap in between each sample swath was a buffer to prevent upslope regolith from caving in downslope when the metal boxes were removed. Any aluminum grains that may have been in these gaps were not collected.

30 mm grains

Upon collection, the long tape was once again laid across the two pieces of rebar. A smaller tape measure was used to measure each pebble's distance moved downslope from its initial position (marked by the long tape) (Fig. 2.4). The lateral distance traveled by each pebble was not recorded.

Figure 2.4. Measuring distance traveled downslope by the 30 mm pebbles.

2.3 Sediment traps

Sediment traps are small devices placed flush with the hillslope surface that can capture flux of regolith movement parallel to the surface (Wells and Wohlgemuth, 1987), useful for determining soil flux of different grain sizes. Sediment flux data were derived from sediment traps experiments conducted by Madoff (2015); the volumes of several different grain size classes were determined by weighing the relative amounts of each grain size that ended up in the sediment traps. Bulk samples were also collected on the hillslopes adjacent to and upslope of the sediment traps. This was done to be able to

compare the relative volumes of different grain sizes in the sediment traps versus the hillslopes.

2.4 Bulk surface regolith sample collection

Bulk regolith samples were collected along each moraine in order to compare the output of the grain size distribution model to observed grain size distributions. Along both the Mono Basin and Tahoe moraine, three bulk samples were collected (using a shovel and bucket): one sample at the crest of each moraine, one sample at the midslope, and one sample at the bottom of each moraine. Samples were taken to a depth of about 10 cm over a roughly circular area about 30 cm in diameter. Each bulk sample weighed approximately 10 kg. A map view of sample locations is shown in Fig. 2.5. Coordinates of each sample location can be found in the Appendix.

Figure 2.5. Bulk sediment sample locations. (A) Sample location on Mono Basin moraine. (B) Sample locations on Tahoe moraine.

2.5 Laboratory sample processing

Aluminum grain samples

To retrieve the aluminum grains within the swath samples, two sieves were used (0.58 mm and 1 mm square openings) to sort for both the 0.7 mm and 3 mm aluminum grains. The aluminum grains have a metallic shine to them which made it possible to simply pick them out by hand (using tweezers). This process was repeated for each sample and the number of grains in each sample was recorded. It is important to note that not all grains initially distributed were recovered, especially so for the 0.7 mm grains. Information on the recovery rates of grain at each site can be found in Table 3.8

Bulk samples

The bulk regolith samples were sieved into the following grain size classes: >63 mm, 27-63 mm, 9.42-27 mm, 4-9.42 mm, 1-4 mm, 0.58-1 mm, <0.58 mm. These sizes were selected based on the availability of certain sieve sizes, as well as the fact that that further divisions were not deemed particularly necessary. The weight of each grain size range was recorded for each of the six bulk samples. For the mathematical modeling part of this experiment, the 0.7 mm grains are associated with the 0.58-1 mm weight class, the 3 mm grains are associated with the 1-4 mm weight class, and the 30 mm grains are associated with the 27+ mm weight classes.

2.6 Mathematical modeling

The computer model created for this study uses a hillslope diffusion equation (Eq. 3) and several new sets of equations that calculate grain size distributions and how they change over the length of the slope (based on the diffusion equation and transport rates of

different grain sizes). The following paragraphs expand on the model operations and parameters.

The hillslope diffusion equation

The hillslope diffusion equation is a combination of two equations: a conservation equation and a transport equation. The conservation equation is as follows:

(Eq. 1) $$-dz/dt = dq/dx$$

This equation says that the rate at which the elevation of a location changes (as material moves downslope) is equal to the difference of the rates that material enters and leaves the location. For example, if more regolith leaves a location than enters, the elevation of that location must decrease. The variable *dz* is the change in elevation (m). The variable *dt* is change in time (years). The variable *dx* is change in horizontal distance (m). The variable *q*, a flux (in this case, flux of the surface regolith, in m^3/m-yr), is calculated using a second equation:

(Eq. 2) $$q = -\kappa(dz/dx)$$

The variable *dz/dx* (m/m) is the slope gradient. Kappa (κ, m^3/m-yr), is a topographic diffusivity constant that modifies the slope gradient. It represents the volume of regolith moving downslope per unit time per unit length transverse to the slope as a result all of the environmental factors that contribute to downslope regolith movement (Hallet and Putkonen, 1994); for example, in an arid region without much precipitation or wind to move particles on a hillslope, one may find a κ value that is smaller than a temperate region that receives much more rain and wind to move particles. Perhaps a region with more animal activity would receive a higher κ value than an identical region

with no animals. Substituting *q* into equation (1) yields the final hillslope diffusion equation:

(Eq. 3) $$dz/dt = \kappa(d^2z/dx^2)$$

This equation gives the rate of change in surface elevation with time as a function of hillslope curvature. It should be noted that this κ value as it stands does not take into account variability in past climate conditions (Madoff, 2015), and assumes the same conditions for the full extent of the time period modeled. The diffusion equation can be applied to any two-dimensional slope data; in this study, it is simulated on moraine slope profiles.

Constructing slope profiles

The dimensions of the sampled Tahoe moraine and Mono Basin moraine are different, and these differences must be accounted for in the model. At locations where bulk sediment samples were taken for this study, the Tahoe moraine is approximately 45 m in height and 100 m from crest to foot, with a maximum slope angle of 27 degrees. The Mono Basin moraine is approximately 50 m in height and 200 m from crest to foot, with a maximum slope angle of 20 degrees. Care must be taken to ensure that the final modeled slope profile closely matches these dimensions to ensure a realistic model. It is also important that the initial profile for both moraines should have a slope angle of 30 degrees, an angle which is considered to be the stable threshold for slopes of granitic origin (Melton, 1965).

Overview of grain parameters

If changes in grain size distribution on slopes over time are to be predicted, we must know the rates at which different grain move along slopes. The hillslope diffusion

model uses the hillslope diffusion equation to slowly degrade hillslopes. Oehm and Hallet (2005) determined that soil creep of regolith can be described by soil flux (κ) and surface soil velocity, and found a positive correlation between the two. The model created for this study uses a transport factor for each grain size, a constant that is meant to represent the downhill transport rate of each grain size. Therefore, the model does not use separate inputs for both surface flux and surface velocity; the transport factor is meant to represent the effects of both.

This model uses four main parameters to calculate grain size distributions along the slope: a depth of the mobile surface layer of sediment; a transport factor (a constant for each grain size that modifies the availability of each grain size to be transported); initial grain size percentages, and a weathering parameter that is applied to only the largest and smallest grain sizes (discussed below).

Modeling the mobile surface layer of regolith

One of the goals of this study was to model the way hillslopes evolve by monitoring the mobile transport layer of regolith resting at the surface of the hillslopes. The depth of the mobile layer of surface may be set by the user within the model; the modeling in this study uses a depth of 10 cm as the mobile layer. This is a reasonable value for depth of the mobile layer: in a study by Oehm and Hallet (2005), the smallest topographic diffusivity they measured (0.01 m^3/m-yr) showed a depth of motion of 9 cm. This is the same topographic diffusivity used to model the Mono Basin moraine, and 2 times that of the topographic diffusivity used to model the Tahoe moraine.

There are three outcomes that may result from sediment transport at any point on the hillslope: addition of surface regolith (deposition), removal of surface regolith

(erosion) or equal addition and removal (no change). For every time step, every point along the slope with a net positive volume undergoes a calculation that combines the new volume with the mobile layer of regolith that was there in the previous time step. The newly added volume and the old volume are re-calculated into a new mobile layer that will be used in the next time step. The relative weight percentage of each grain size is monitored during this calculation. Alternatively, every point on the slope with a net negative volume undergoes a calculation that removes a portion of the mobile surface layer and adds new regolith from underneath to maintain the depth of the mobile layer. Again, the relative weight percentage is monitored for each grain size during this calculation.

Transport factor

The total κ-values for each moraine were determined by testing different κ-values in the diffusion equation and finding the value that resulted in the closest match to the moraine profile of the present day. The total κ-value that provided a best match for the current Tahoe moraine profile (45,000 years) was 5×10^{-3} $m^3/m/yr$. The total κ-value that provided a best fit for the current Mono Basin moraine profile (100,000 years) was 1×10^{-2} $m^3/m\text{-}yr$. The κ-value value by itself is considered to be an intrinsic property of the material and is a constant, but can fluctuate over time due to varying climactic conditions (Madoff, 2015), which might explain why the κ-values for both moraines are slightly different. Both κ-values come close to the κ-value determined by Putkonen and Hallet (1994) for the past 22,000 years, which was 1.2×10^{-2} $m^3/m/yr$.

For each time step, each point along the slope has a net volume entering or leaving based on the diffusion equation. The volume is divided into different grain sizes

based on the transport factor of each grain size and its availability at the surface. This is important because it limits the amount of a certain grain size that can be transported based on its presence in the mobile layer of regolith; for example, if a point on the slope has no 27+ mm grains present, even if the transport factor of the 27+ mm grains is not zero, none will be transported since it is not available to be transported.

Initial grain size distribution

The initial grain size distribution of each grain size class is able to be adjusted within the model parameters. It is difficult to determine, with certainty, the original grain size distributions within the moraines. Intuition may say that the crest of the youngest moraine should reflect the original distribution of the moraine, because regolith is getting freshly exposed as the material above it erodes away. This may be true, but it also does not take into account processes like the weathering of larger clasts into smaller ones, which may cloud traces of the original distribution.

Weathering

It is important to consider weathering when modeling hillslope grain size composition; the gradual breakdown of rock into smaller sizes will have some effect on the final grain size distribution of the hillslope. Breakdown of grains into smaller sizes is a complicated process and little is known about the rates at which certain grain sizes break into smaller sizes. A study by Putkonen and others (2014) modeled the way boulders weathered into smaller fragments, but does not explore weathering of grains smaller than 5 mm, which make up a majority of the regolith volume in this study. Other studies (Caine, 1974; Dixon et al., 2001) have measured the rates of annual weight loss of

small (<6 mm) granitic grains, but these studies only examine the chemical weathering rates of grains and do not discuss the breakage of grains into smaller particles.

To simplify the weathering phenomenon within the model, the largest grain size is assigned a weathering parameter that degrades a small percentage of its volume into the smallest grain size for each time step. The logic behind this is that there are five different grain size classes; each should partially break down into the grain size smaller than it. Instead of simulating the transfer of material through five different grain size classes, this instead directly transfers coarse (27+ mm) material into fine (<0.58 mm) material, since the largest grain size class should always be losing mass and the smallest grain size class should always be gaining mass. Of course, it is possible that different size grains weather differently due to surface area exposure or the scale at which fractures appear. However, due to a lack of concrete data for all grain sizes, this simplified process is used. The weathering constant that can be applied in this model is a certain percentage of volume per year. The weathering rate is applied to both surface and subsurface material for the duration of the model.

Theoretically, a combination of four parameters (transport factor, initial grain size distribution, depth of mobile layer, and weathering rate) will concentrate certain grain sizes on certain parts of the slope within the specified surface layer of regolith. As time progresses, the presence of certain grain sizes may change as the model continually runs. The objective of the modeling is to generate a figure showing the weight percentage of each grain size class along the entire hillslope at any point in time.

Mathematical modeling for this project was done using MATLAB R2017a. MATLAB code is found in the Appendix.

CHAPTER III

DATA

3.1 Rainfall measurements

Measured rainfall for the region was a 1.65 cm for the 101-day span. The precipitation data come from a National Weather Service weather station located in Lee Vining, CA. Day-by-day weather data can be found in the Appendix. All field sites were located within 6-9 km from the Lee Vining weather station. The annual average rainfall at this weather station over the past 30 years (as far as the data go back to) was measured to be 6.3 cm, approximately four times more than the amount of rainfall measured over the study period.

3.2 Grain transport rates

Aluminum grains (0.7 mm and 3 mm) from each swath downslope of the initial placement were counted and the number of grains in each sample was recorded. The maximum possible transport distance of each grain was considered to be the furthest downslope end of the metal box it was collected in. The minimum possible transport distance of each grain is the upslope edge of the metal box it was collected in. The average transport distance is considered to be the middle of the metal box it was collected in. The distance that each 30 mm pebble traveled was also measured and recoded. The data gathered from these measurements are displayed in Tables 3.1-3.6.

Table 3.1. Transport distances for 0.7 mm and 3 mm grains on a 14 degree slope angle.

AG-MBO-1-2017	Slope angle: 14 degrees			
Distance traveled (cm) (min)	Distance traveled (cm) (max)	Distance traveled (cm) (average)	0.7 mm grains recovered	3 mm grains recovered
200	208	204	0	0
165	173	169	0	0
130	138	134	0	0
100	108	104	1	0
90	98	94	0	0
80	88	84	3	1
70	78	74	1	0
60	68	64	1	0
50	58	54	4	0
40	48	44	2	0
30	38	34	1	1
20	28	24	22	3
10	18	14	212	11
0	8	4	1002	55
0	0	0	888	22

Table 3.2 Transport distances for 30 mm pebbles on a 14 degree slope angle.

PB-MBO-1-2017	
Pebble #	Distance downslope (cm)
1	0
2	8
3	0
4	1
5	0
6	0
7	0
8	0
9	0
10	0
11	0
12	0
13	0
14	0
15	0
16	0
17	0

Table 3.3. Transport distances for 0.7 mm and 3 mm grains on a 20 degree slope angle.

AG-MBY-2-2017	Slope angle: 20 degrees			
Distance traveled (cm) (min)	Distance traveled (cm) (max)	Distance traveled (cm) (average)	0.7 mm grains recovered	3 mm grains recovered
200	208	204	0	0
165	173	169	0	0
132	140	136	1	0
98	106	102	10	0
80	88	84	14	0
60	68	64	8	0
50	58	54	34	1
40	48	44	34	1
30	38	34	41	3
20	28	24	124	7
10	18	14	120	11
0	8	4	616	12
0	0	0	402	24

Table 3.4.Transport distances for 30 mm pebbles on a 20 degree slope angle.

PB-MBY-2-2017	
Pebble #	Distance downslope (cm)
1	6
2	2
3	1
4	0
5	1
6	0
7	1
8	0
9	8
10	0
11	15
12	10
13	0
14	0
15	2

Table 3.5. Transport distances for 0.7 mm and 3 mm grains on a 27 degree slope angle.

AG-MBY-3-2017	Slope angle: 27 degrees			
Distance traveled (cm) (min)	Distance traveled (cm) (max)	Distance traveled (cm) (average)	0.7 mm grains recovered	3 mm grains recovered
200	208	204	0	0
165	173	169	0	0
130	138	134	0	2
100	108	104	1	1
90	98	94	4	3
80	88	84	3	0
70	78	74	3	10
60	68	64	5	9
50	58	54	20	1
40	48	44	40	3
30	38	34	42	0
20	28	24	160	38
10	18	14	1346	13
0	8	4	431	1
0	0	0	8	0

Table 3.6 Transport distances for 30 mm pebbles on a 27 degree slope angle.

PB-MBY-3-2017	
Pebble #	Distance downslope (cm)
1	0
2	3.5
3	2
4	10
5	5
6	15
7	37
8	0
9	15
10	0
11	10
12	8.5
13	0
14	4
15	17

Table 3.7. Compiled transport distances from all grain sizes at all sites. Average transport distance calculated by averaging the transport distance of each grain using the distance in the "Distance traveled" (average)" column in the above tables.

0.7 mm grains		
Site	Slope Angle (°)	Avg. transport distance (cm)
AG-MBO-1-2017	14	3.901
AG-MBY-2-2017	20	10.463
AG-MBY-3-2017	27	14.518
3 mm grains		
Site	Slope Angle (°)	Avg. Transport distance
AG-MBO-1-2017	14	6.065
AG-MBY-2-2017	20	9.661
AG-MBY-3-2017	27	40.173
3 cm pebbles		
Site	Slope Angle (°)	Avg. Transport distance
PB-MBO-1-2017	14	0.529
PB-MBY-2-2017	20	3.067
PB-MBY-3-2017	27	8.467

Table 3.8. Percent of grains of each grain size recovered at each field site.

	% Grains Recovered		
Grain size	14° slope angle	20° slope angle	27° slope angle
0.7 mm	71	47	69
3 mm	93	59	81
3 cm	100	100	100

3.3 Bulk regolith samples

Mono Basin Moraine

The regolith at the foot of the Mono Basin moraine was dominated by grains finer than 0.58 mm, with decreasing weight percentages of grains coarsening upwards (with a spike at the 1-4 mm grain size bin). Regolith at the midslope of the moraine exhibited a

similar pattern, but with a slightly larger percentage of coarser grains, especially in the 1-4 mm range. The crest of the moraine continued this pattern, but with an increased amount of grains within the 9.42 – 27 mm grain range (Fig. 3.1).

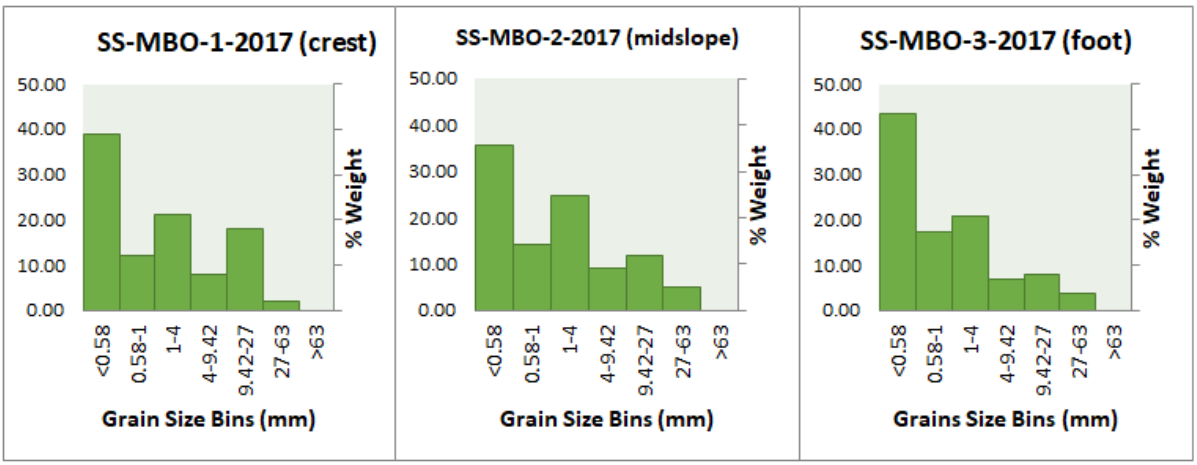

Figure 3.1. Histograms for bulk sediment samples on the Mono Basin moraine.

Tahoe Moraine

The regolith at the foot of the Tahoe moraine was mostly composed of grains in the <0.58 mm range and the 1-4 mm range. At the midslope, the distribution is similar with the exception of an increased amount of the coarsest grain size measured (>27 mm). The crest of the moraine was dominated by grains <0.58 mm and grains >27 mm (Fig. 3.2).

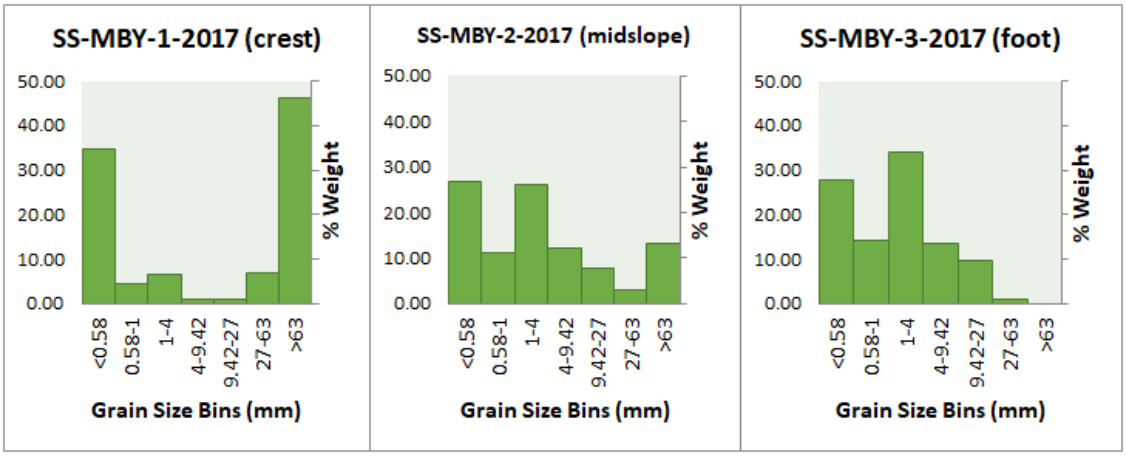

Figure 3.2. Histograms for bulk sediment samples on the Tahoe moraine.

Measurements from the sediment traps showed that in all traps, the weight percent of the grains between 1.19 and 4 mm exceeded the weight percent adjacent to the traps. The relative percent differences for the other grain size classes were much more varied between samples, with high standard deviations.

Table 3.9. Sediment trap measurements from 5 sediment traps on the Tahoe and Mono Basin moraines.

	Weight % in sediment trap minus weight % on adjacent hillslope					
ST-MB-1-2010	4.3	2.4	2.1	2.9	14.5	-26.1
ST-MB-2-2010	-6.4	2.0	6.4	7.1	27.2	-36.3
ST-MB-3-2010	-18.8	0.0	0.5	2.5	-12.7	28.6
ST-MB-4-2010	3.3	13.8	5.5	4.5	-14.7	-12.4
ST-MB-5-2010	15.5	12.4	7.4	1.1	-20.2	-16.2
Avg. Percent Difference	-0.4	6.1	4.4	3.6	-1.2	-12.5
Grain size (mm)	0 - 1.19	1.19 - 1.68	1.68 - 2.83	2.83 - 4	4 - 10	10 -16

CHAPTER IV

RESULTS

4.1 Overview

The objective of the present study was to determine transport rates of different grain sizes and determine how this affects grain size distribution along the slope over time. Transport rates for different grain sizes were determined by measuring both surface velocity and volumetric flux of different grain sizes over known time periods. A model was created to accommodate a transport factor that is meant to reflect these transport rates. This diffusion-based hillslope degradation model is based on the hillslope diffusion equation, with varying grain size parameters for depth of mobile layer, transport factor, weathering rate, and initial grain size distribution. The model is meant to predict the grain size distribution along the length of the hillslope over a period of time.

4.2 Transport rates of individual grains

The pattern of transport downslope for the 0.7 mm, 3 mm, and 30 mm grains is shown in Figure 4.1. There is a clear trend of increasing transport distance with increasing slope angle, as well as differentiation of transport distances between grain sizes. It appears that on shallower slopes, there are smaller differences between transport distances of different sized grains, while on steeper slopes, differences in grain transport distance are evident.

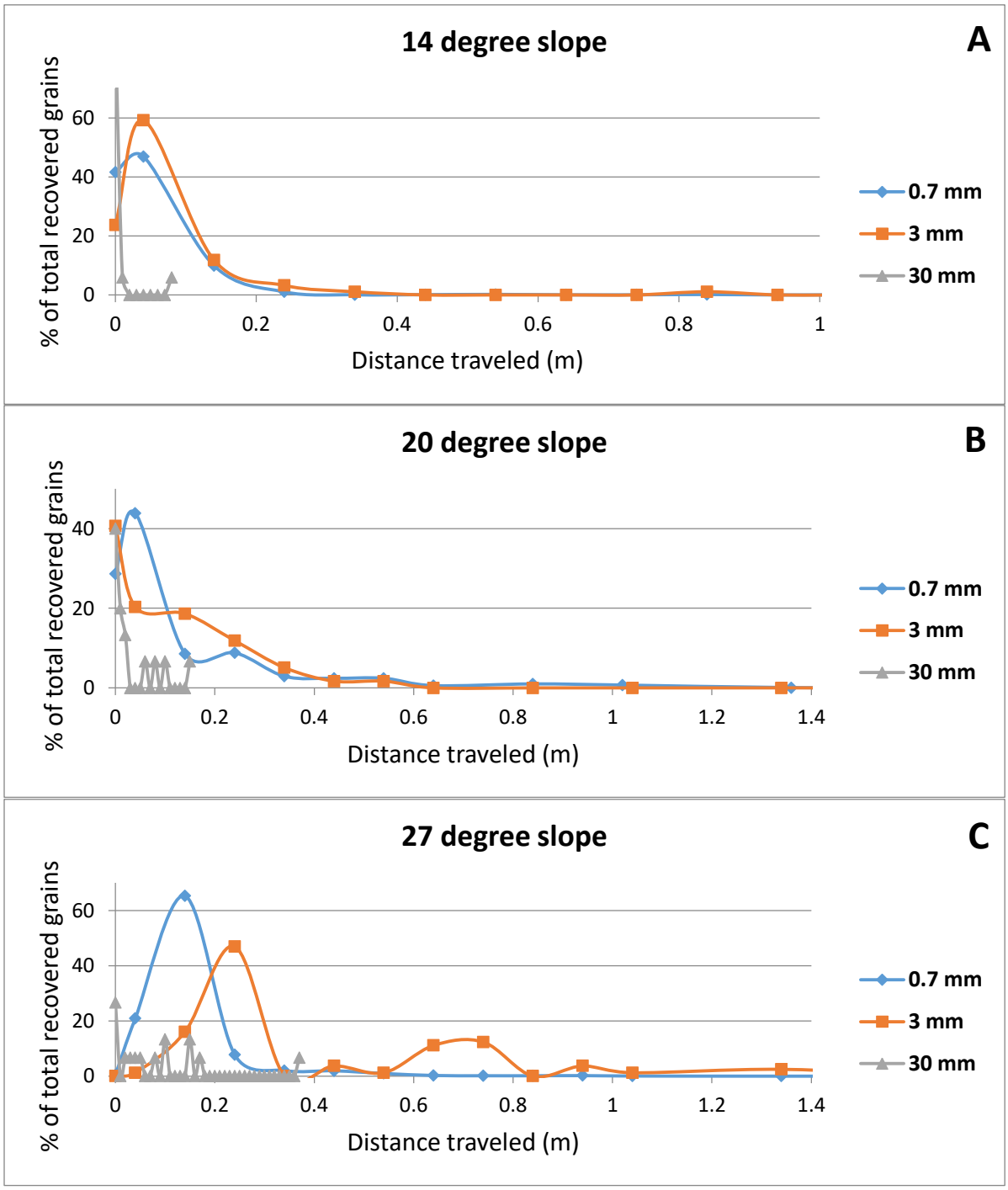

Figure 4.1. Distribution of 0.7 mm, 3 mm, and 30 mm grains downslope of initial placement. X-axis shows distance from initial area of distribution. Y-axis shows the percent of grains recovered for that grain size. 3,000 0.7 mm grains, 100 3 mm grains, and 15-17 30 mm grains were initially dispersed at each site. (A) Data for site MBO-1-

2017 (14 degree slope angle). (B) Data for site MBY-2-2017 (20 degree slope angle). (C) Data for site MBY-3-2017 (27 degree slope angle).

At site MBO-1-2017 (14 degree slope), the average transport distance of the 3 mm grains was the highest, followed by the 0.7 mm grains, followed by the 30 mm pebbles. At site MBY-2-2017 (20 degree slope), the average transport distance of the 0.7 mm grains was the highest, closely followed by the 3 mm grains, and followed by the 30 mm pebbles. At site MBY-3-2017 (27 degree slope), the average transport distance of the 3 mm grains was by far the highest, followed by the 0.7 mm grains and the 30 mm pebbles (Fig. 4.2).

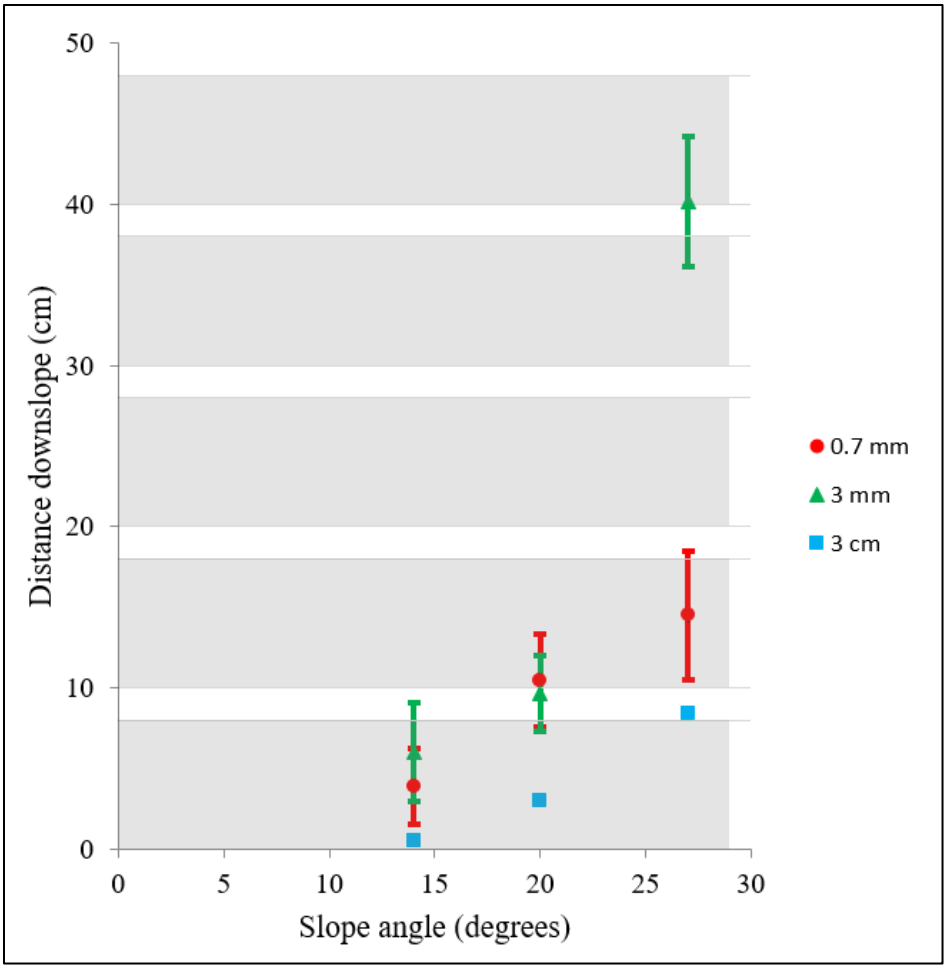

Figure 4.2. Grain transport distances for all three field sites. Data points in the graph represent average transport distance of all grains, assuming all grains ended up in the center of the swaths they were collected in. For example, if a grain was collected in the 10-18 cm downslope range, it was assumed to have traveled 14 cm. Upper error bars represent the average transport distance of all grains, assuming they all traveled to the furthest downslope part of the metal boxes they were collected in. Lower error bars represent the average transport distance of all grains assuming they all traveled to the furthest upslope part of the metal boxes they were collected in. The 30 mm grains do not have error bars because they were not measured using the metal box method; their transport distances were able to be measured directly. The gray shaded areas show the upper and lower extents of said metal boxes for reference.

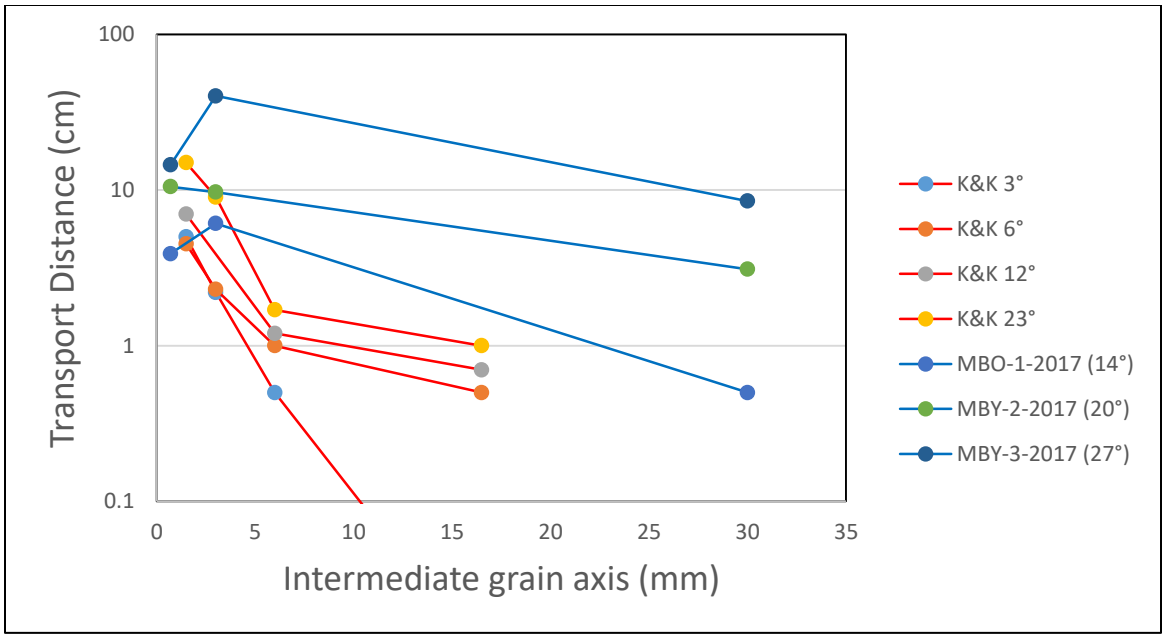

Figure 4.3. A comparison between grain transport distances vs. grain size in this study (MBX-X-2017) and Kirkby and Kirkby (1974) (denoted by "K&K").

Figure 4.3 shows a comparison between the grain transport data in this study versus that of Kirkby and Kirkby (1974). There is a clear trend in the other study of increasing transport distance with decreasing grain size. This trend is reflected in the larger grain sizes (from 30 mm to 3 mm) for this study, but the trend from 1 mm to 0.7 mm grains shows anywhere from a very minor increase in transport rate to a somewhat sharp decrease. One explanation for this difference is that 3 mm grains do in fact travel faster than 0.7 mm grains across the surface, and that the trend of increasing velocity with grain size stops as grains reach around 1 mm in diameter. While intuitively this seems unlikely, it is possible that smaller grains are more susceptible to sticking together with other small grains under wet conditions or becoming trapped between larger grains, limiting their velocity during mobilization events. It is also possible that some part of the 0.7 mm grain transport was lost due to sampling error. Recall that 11-22% less 0.7 mm

grains were recovered during collection of grains at the field sites compared to 3 mm grains, and that a maximum of 70% of the 0.7 mm grains were recovered at any field site. The portion of the 0.7 mm grains not accounted for may have traveled past the extent of the distance downslope sampled (~2 m). This seems very unlikely since the transported plume of grains tails off convincingly at each site, i.e. there would have to have been a large mass movement of grains that traveled a suspiciously long distance downslope. The other reason for unrecovered grains may be that they got buried deeper than the depth of sampling (5 cm).

To address this further, a brief laboratory experiment was conducted to see if the results could be replicated. Regolith from the midslope of the Tahoe moraine was spread about 5 cm deep in an aluminum pan and angled to 27 degrees to mimic the field conditions at which the 3 mm grains traveled much further than the 0.7 mm grains. 10 of each size of the aluminum grains (3 mm and 0.7 mm) were placed in a line across the surface of the regolith. A mesh screen was mounted above the grains, and rainfall was simulated by slowly releasing drops of water from 4 pipettes at the same time above the mesh (the mesh acted to disperse the larger droplets coming out of the pipettes), with care taken to evenly distribute water over all of the grains. About 50 mL of water was released from the pipettes for the simulation. This simulation was attempted 3 times. The first 2 simulations showed no movement of any grains, with full burial of several of the 0.7 mm grains due to rain splash and partial burial of several 3 mm grains. The third simulation showed slight movement of two 3 mm grains (2-3 mm downslope) and slight movement of one 0.7 grain downslope (10 mm). In all tests, the rainfall seemed to stabilize the grains rather than mobilize them. A fourth test was conducted to attempt to better

mobilize the grains: water was pipetted directly upslope of a line of 10 grains of each grain size. It was pipetted until a portion of regolith became saturated to the point of collapsing downslope. For both grain sizes, 2 grains were mobilized and in both cases moved about 20 mm downslope. In any case, rainfall did not seem to differentiate the transport distances of the different grain sizes.

Recall that in the field experiment, the 3 mm grains were placed directly upslope of the 0.7 mm grains, and that the 0.7 mm grains experienced burial from rainsplash in the laboratory test. In the field setting, it is possible that the 0.7 mm grains placed were initially shallowly buried in the mobile portion of the regolith at the surface from rainsplash or small-scale events of bulk movement. Since the 3 mm grains are not buried as easily, they may have been able to subsequently travel downslope along the surface when the 0.7 mm grains were still buried. Larger grains may have a natural buoyancy that allows them to stay at the surface more easily and move during rainfall events. It could potentially be that smaller grains travel faster when moving at the surface, but are not present at the surface as often as larger grains, so that over certain time periods it appears that larger grains travel faster.

While placing the grains on the dry, sloped regolith in this laboratory test, it should be noted that the 3 mm grains had a tendency to tumble down the slope even when gently placed on the surface. The 0.7 mm grains did not exhibit this behavior. This indicates that on a dry surface, 3 mm grains may be more unstable and travel further than 0.7 mm grains. However, events that mobilize grains on dry surfaces are either somewhat uncommon or sporadic (animal activity) or do not provide much energy with which to move grains (wind).

4.3 Sediment traps

The sieved regolith within the sediment traps was compared with the sieved regolith from the surface of the hillslope immediately upslope of the sediment traps. For the grain size class from 1.2 – 4.0 mm, the average difference in the weight percent in the sediment traps versus the weight percent on the adjacent hillslope was positive. The smaller and larger grain size classes showed an average negative difference. This result indicates that the 1.2 – 4.0 mm grains may have the highest downslope transport rate. It is important to note that the variance in the results of the 0 – 1.2 mm and 4 – 16 mm diameter grains was much higher.

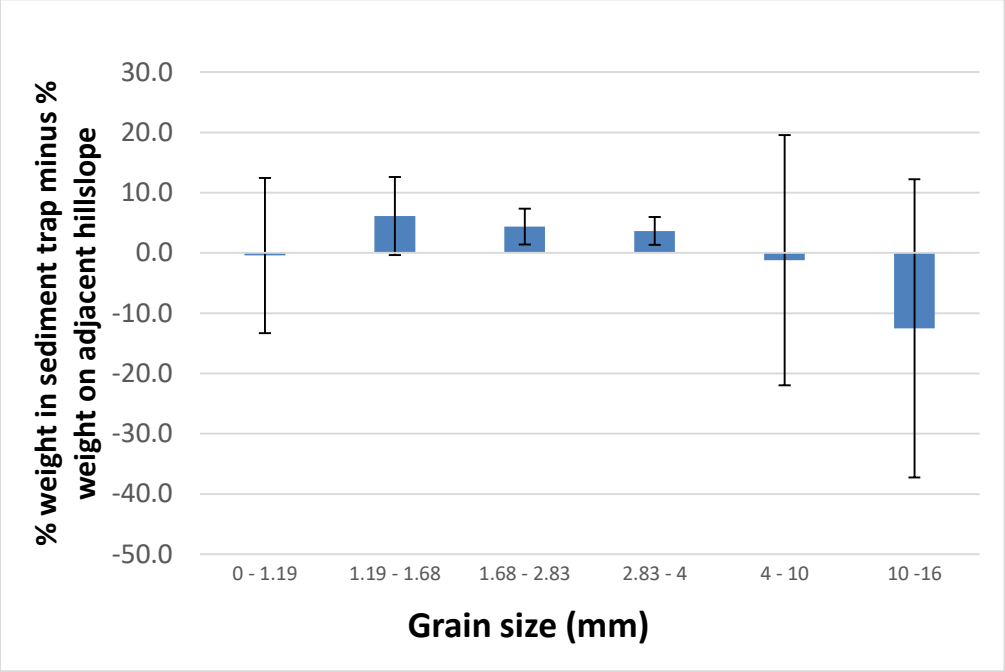

Figure 4.4. Percent weight of certain grain size classes in sediment traps minus percent weight of certain grain size classes on hillslopes adjacent to sediment traps. Error bars represent one standard deviation. Data derived from 5 sediment traps: 3 on the Tahoe moraine midslope, 2 on the Mono Basin moraine midslope.

4.4 Mathematical modeling

It is now necessary to find a certain set of starting parameters that best match against the observed grain size distributions sampled along the hillslopes. To calculate a best fit, different combinations of starting parameters were inserted into the model, and the sum of the squared residuals was calculated by the model by finding the difference between the modeled grain size distribution and the observed grains size distribution. The squared residuals were averaged between footslope, midslope, and crest locations on both the Tahoe moraine (45,000 years) and the Mono Basin moraine (100,000) years. The best fit was determined to be the smallest of the averaged squared residuals for the model runs (least square).

Table 4.1. Starting parameters for the best fit model.

Grain size	**% of sum of transport rates**	**% Initial weight**
<0.58 mm	22	10
0.58-1mm	22	10
1-4mm	24	20
4-27mm	22	20
27+mm	9	40
Weathering rate: 0.002%/year	Total κ: 0.005 & 0.01 m^3/m-yr	
Duration: 45,000 and 100,000 years	Mobile layer: 10 cm	

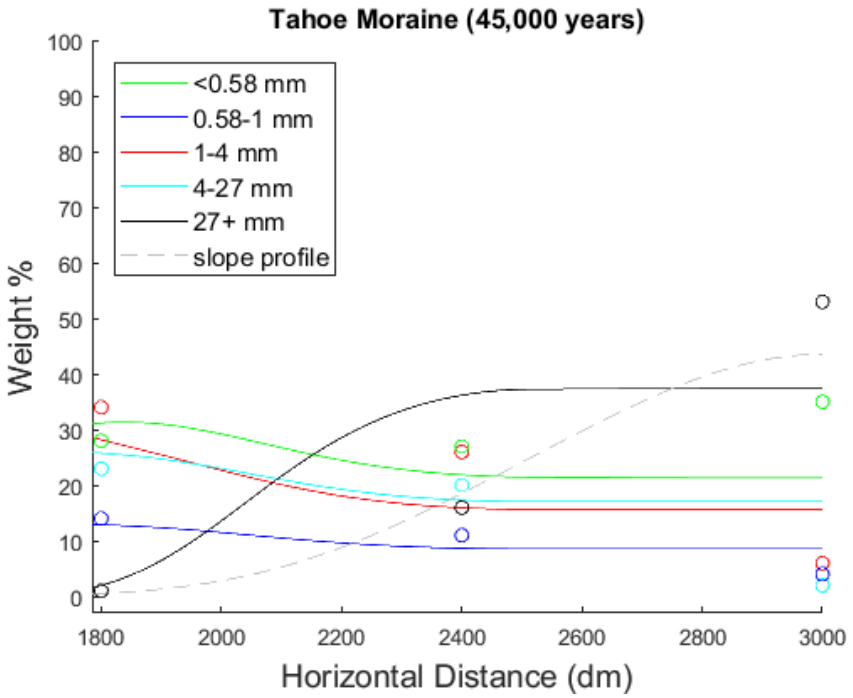

Figure 4.5. Modeled grain size distributions along the Tahoe moraine after 45,000 years under the conditions in Table 4.1. The colored dots represent the observed grain size weight percentages at that place on the slope (Fig. 3.2). The dashed line is the moraine profile at the end of the simulation.

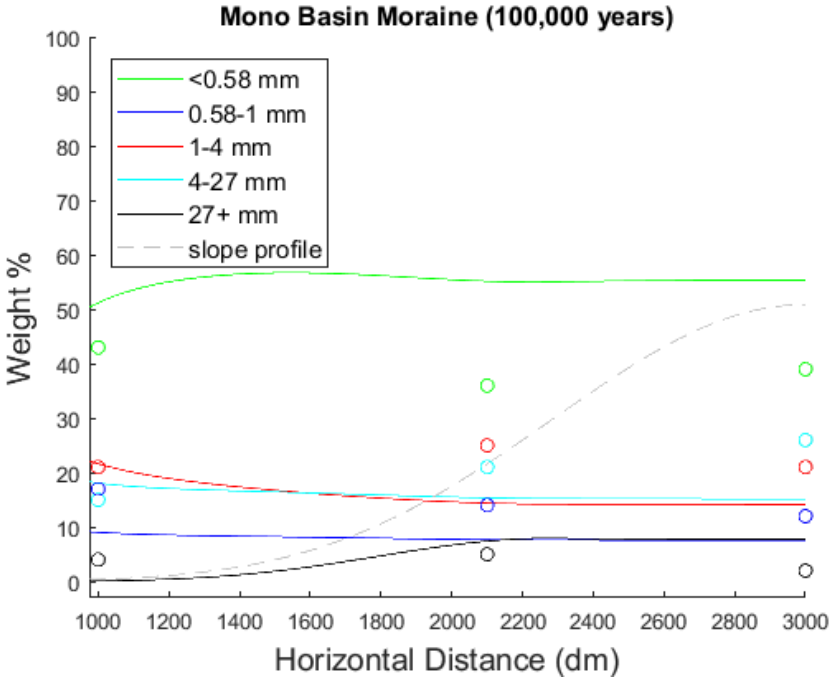

Figure 4.6. Modeled grain size distributions along the Mono Basin moraine after 100,000 years under the conditions in Table 4.1. The colored dots represent the observed grain

size weight percentages at that place on the slope (Fig. 3.1). The dashed line is the moraine profile at the end of the simulation.

The model was able to fairly accurately predict the footslope grain size distribution under the parameters given. The model is slightly less accurate in exactly predicting the grain size distribution on the crest, but still captures the general trend. The model is least accurate in predicting the grain size distribution on the midslope of the Tahoe moraine, mainly for the 1-4 mm grains and the 27+mm grains. (Fig. 4.9, 4.10).

It is important to note that the differences between the final outputs of the Tahoe and Mono Basin models are almost entirely due to the weathering constant applied. The weathering constant that provided the best fit was 0.002%. Within this model, this means that annually there is a 0.002% decrease of the largest grain size class (27+ mm) and a 0.002% increase in the smallest grain size class (<0.58 mm). Without the weathering constant, the modeled output, for both moraines, reaches a steady state after about 5,000 years and has very little change thereafter. Weathering is the major time-dependent factor of the difference in grain size distributions for both moraines, assuming all other parameters remain the same for both moraines.

Consistent with both model outputs is the fact that above the midslope, grain size distributions remain relatively unchanged. This appears to be true in reality for the Mono Basin moraine; in fact, the entire moraine contains a similar distribution. The Tahoe moraine does not share the same monotone distribution.

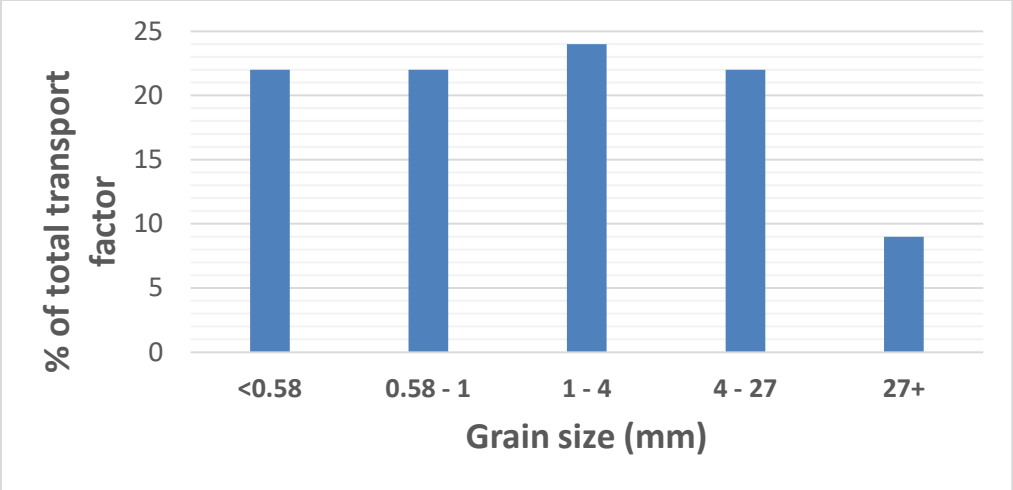

Figure 4.7. Transport factors for certain grain size classes that provided the best fit within the model to the observed grain size distributions. The total transport factor is the sum of all transport factors.

The best fit transport factors for the grains showed that the grains within the 1-4 mm grain size class exhibit the highest transport rate. This result is consistent with the results of the individual grain transport experiment, which showed the 3 mm diameter grains having the highest transport rate. It is also consistent with the results of the sediment traps experiment, which showed grains within the 1.2 – 4.0 mm grain size class as having the highest transport rate.

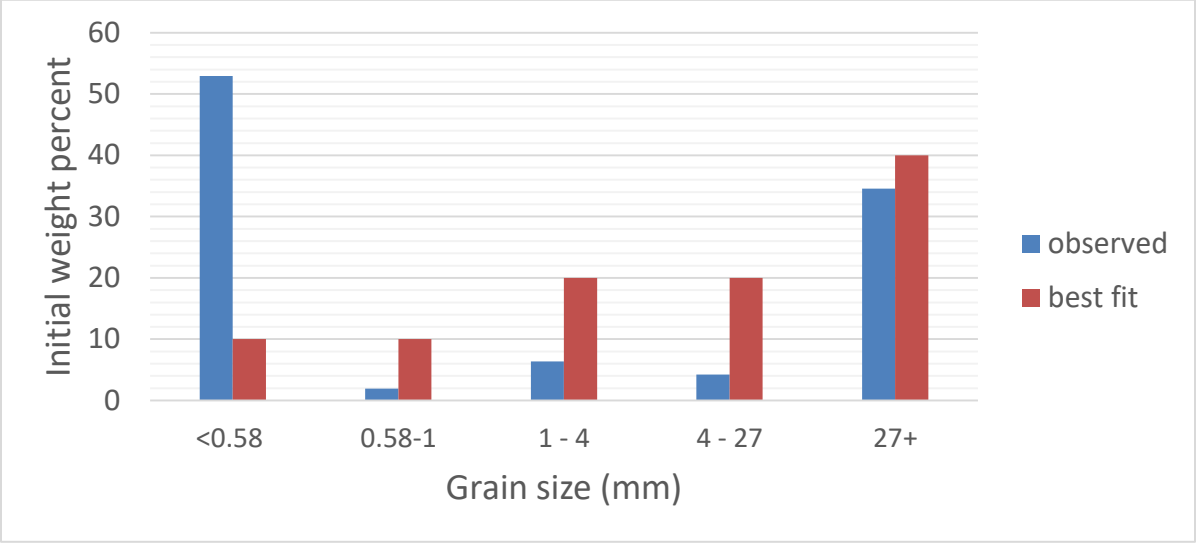

Figure 4.8. Observed initial weight percent of each grain size vs. initial weight percent used in the best fit model.

The observed initial weight percent was assumed to be the grain size distribution of the crest of the Tahoe moraine, where there is a vast majority of a mixture of very fine (<0.58 mm) sediment and large (27+ mm) cobbles. This distribution did not match well to the smaller grain size classes, and had a close fit to the 27+ mm grain size class.

In addition to observing how grain size distribution changes spatially, the model can be used to see how grain size distribution changes over time at a certain fixed point on the landscape. Using the best fit parameters, the model was run to see how grain size distribution changed at the crest and the footslope over time. It is important that along with a spatial prediction of grain size distributions, we also have a way to easily assess temporal changes in grain size distribution at any point on the slope. The below figures (Fig 4.16, Fig. 4.17) are results of modeling the grain size distributions at the crest and footslope over time. Knowing the way grain size distribution changes over time can allow predictions to be made about slope stability (certain distributions and lithologies are more

stable than others on slopes), as well as predict how regolith is arranged in the subsurface.

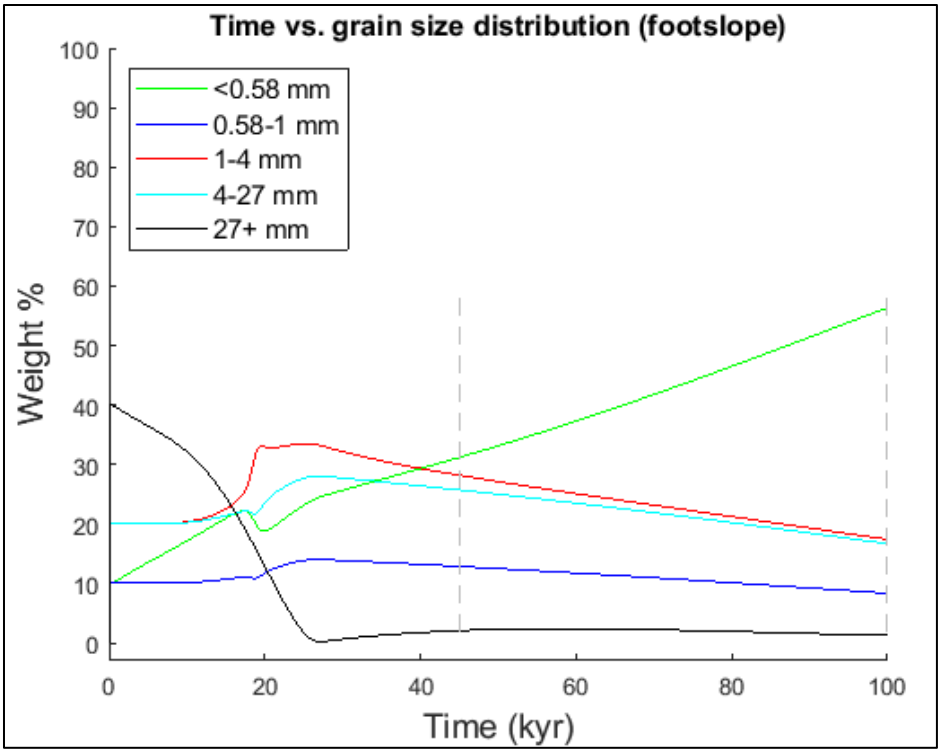

Figure 4.9. Time versus the change in weight percent of different grain size classes at the footslope of the Tahoe and Mono Basin moraines. The gray dashed lines indicate the time after deposition for each moraine.

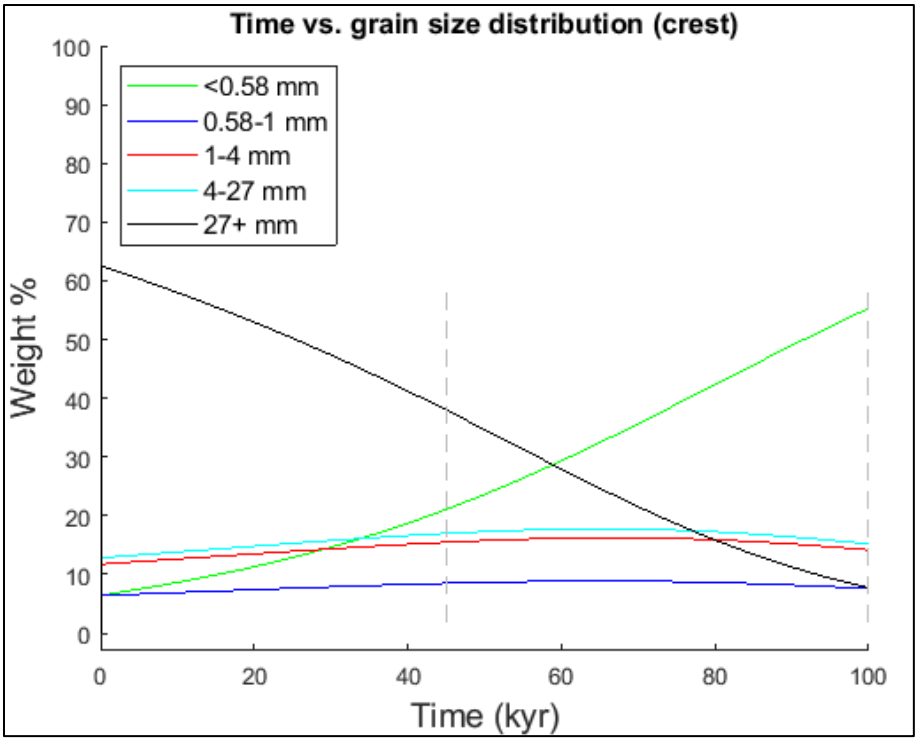

Figure 4.10. Time versus the change in weight percent of different grain size classes at the crest of the Tahoe and Mono Basin moraines. The gray dashed lines indicate the time after deposition for each moraine.

CHAPTER V

DISCUSSION

5.1 Overview

A diffusion-based transport model was developed as a way to predict grain size distributions along a moraine slope. The model was built to accommodate a) depth of a mobile layer of regolith, (b) a transport factor for various grain sizes, c) an initial grain size distribution, and (d) a weathering rate. The output of the model was to be tested against the grain size distribution of bulk regolith samples collected along a moraine slope. In this section, the factors that contribute to regolith transport will be re-evaluated. Additionally, the results of the field observations, modeling results, and the differences between them, will be interpreted. Based off of these interpretations, a plausible explanation for the grain size distributions seen on the Tahoe and Mono Basin moraines will be given.

5.2 Direct contributing factors to regolith transport

In reality, there are two ways by which sediment transport downslope can be measured; surface velocity and soil flux. Soil flux of different grain sizes is dependent on both the velocity of the grains as well as the availability at the surface; the volume able to be transported is dependent on the volume available in the mobile layer. The hillslope diffusion model simulates the movement of certain volumes of regolith downslope—

therefore, velocity of different grains cannot be directly applied. For this reason, we use a transport factor within the model and combine it with surface availability to simulate grain movement downslope. This transport factor is a constant for each grain size, and indirectly represents a velocity by which grains travel at the surface. Modeling using grain surface velocities directly may be more suited to a model that can discretely move individual grains and keep track of where each grain is on the hillslope at all times. This type of model would be quite computationally heavy, especially if it was required to individually track a large number of very fine grains.

5.3 Secondary contributing factors to regolith transport

In the model there are three factors that do not directly move regolith at the surface: initial grain size distribution, surface availability, and weathering. The material that is moved by the transport factor is also dependent on these three factors. The initial grain size distribution of the moraine is critical, as the regolith unearthed at the upper slopes and crest of the moraine is the material that eventually gets deposited along the slope surface. If there is a lack of a certain grain size being unearthed (initial composition), this availability should be reflected in the grain size distribution along the hillslope. Additionally, if weathering is occurring, it is making certain grain sizes available that were not available previously.

5.4 Comparison between observed transport rates and best fit transport rates

The best fit model's transport factor values for each grain size showed a correlation to the transport rates measured in the field experiments; in both cases, grains

in the ~1-4 mm grain size range had the highest transport rate, followed by the smallest grains (< 1 mm in diameter), followed by grains larger than 4 mm in diameter.

One interesting observation is that at the footslopes of the both moraines, the measured weight percentages of each grain size generally follow the same trend as the modeled best fit transport factors. The lowest transport factor (27 mm+ grains) is the lowest by weight percent; the second lowest κ value (0.58-1 mm grains) is the second lowest by weight percent, and so on. Theoretically, one could take samples at the base of all moraines in this region and find a similar grain size distribution, if a) the same processes dictate how the grains are transported and weathered and b) the initial grain size distribution for all of the moraines is similar. The following two sections will attempt to describe the process leading to the current grain size distributions of both the Tahoe and Mono Basin moraines, using interpretations from field measurement and results from the best fit of the model.

5.5 The Tahoe moraine

The largest discrepancy in the best fit parameters in the model versus the observed values is the grain size distribution of the material originally deposited. One of the reasons for this occurrence may be the assumption that the crest of the Tahoe moraine is a close match to the original grain size distribution. If the observed distribution on the crest is in fact the original distribution, one must wonder where the intermediate grain sizes come from that are heavily present on the lower slopes of the moraine. One explanation may be that the 27+ mm portion of the crest weathers rapidly, and all smaller grains quickly move off of the crest of the moraine and are deposited on the lower slopes.

This would indicate that the transport rates of the intermediate grain sizes are the largest, especially the 1-4 mm grains that are equally or more present than the <0.58 mm grains on the midslope and footslope. The higher measured transport rates of the 1-4 mm grains and the 4-27 mm grains support this possibility.

Another explanation that rather supports the initial distribution predicted by the best fit of the model is that initially there are few smaller grains (<1 mm) and over time, weathering slowly breaks all larger grains down, producing the relatively high weight percent of <1 mm grains present on the entire extent of the moraine that is seen today. However, that would again mean that the <0.58 mm grains have a lower transport rate than all but the largest grains, as they are still present in large quantities at the crest. In both scenarios, it seems that the 1-4 mm grain size class must have the highest rate of transport. A third possibility could be that some of the <0.58 mm grains are not native to the moraine but instead were transported to the moraine crest through eolian means.

A reason for the apparent lower mobility of the <0.58 mm grains may be that they adhere to each other during precipitation events and become a cohesive surface that allows some larger grains to move on top of them at a more rapid rate. There is also the possibility that the bulk sample collected at the crest of the Tahoe moraine happened to be in a spot that was unusually dense with either the <0.58 mm grains and the 27+ mm grains.

5.6 The Mono Basin moraine

The surface of the Mono Basin moraine carries a similar distribution of grain sizes at the footslope, midslope, and crest at the present day. This is in sharp contrast to

the variable grain size distribution along the surface of the younger and steeper Tahoe moraine nearby. Assuming the same grain size distribution as the Tahoe moraine when it was deposited, any difference in its surface grain size distribution must come from its a) older age or b) shallower slope angles, if we assume that other parameters (transport factor and weathering rates) are held constant between both moraines. Increased age will result in weathering and a decrease in slope along the moraine. A decrease in slope along the moraine will result in a decrease in volume moving down the moraine slopes (per the diffusion equation), and a decrease of exhumation of new material at the moraine crest. As a constant, the transport factors of each grain size are assumed to stay the same regardless of the slope angle.

Both the model and observed transport rates for grains indicate that the 1-4 mm grain size class has the highest transport rate. If this is the case, we should expect the footslope the have the highest percentage of 1-4 grains, by weight, compared to all other grain sizes. However, we see that this is not the case; it is the fine grains (<0.58 mm) that have the highest weight percentage at the footslope. Weathering may offer an explanation for this. The weathering that occurs from the age of the Tahoe moraine to the age of the Mono Basin moraine must break down the material on the surface into smaller grains. The net effect of this weathering should be an increase in the smallest grain size and a decrease in the largest grain size. It is less apparent what happens to intermediate grain sizes during weathering, as they are gaining and losing mass constantly.

What does this mean for the future surface of the Mono Basin moraine (and all moraines in the region)? If the observed trend continues, the average grain size will continue to fall as weathering continues. The grain size distribution along the slope

should also become more similar from footslope to crest, as transport processes for all grains become more similar at lower slope angles. Drawing the trend to its ultimate conclusion, the surface of the moraine should eventually become a homogenous fine sandy silt with no obvious difference in grain size distribution along the surface.

CHAPTER VI

CONCLUSIONS

Landforms change over time in response to erosional processes. The way in which these changes occur can provide insights into the processes that cause them. Knowledge of sediment transport rates can be applied to practical issues within land management as well as help to answer scientific questions about ages of landforms and past climates.

Not only do the general forms of landscape features change in response to erosion; the grain size distribution of surface material changes as well. Grain size distribution is important both as a tool for geologic interpretation and as an indicator for landform stability. Varying grain size distributions along hillslopes are partially the result of varying transport rates between grain sizes. The reasons for varying grains size distributions along hillslopes have not been well-explored, due to the variables that must be taken into account. To be able to predict how grain size distribution changes, the transport rates of differing grain sizes must be known, as well as the initial grain size distribution and weathering rate. There have been attempts to characterize transport rates of varying grain sizes in the past, which have generally shown that transport rate increases with decreasing grain size.

In this study, regolith transport rates and grain size distributions on hillslopes in the Mono Basin region of the Sierra Nevada were measured to understand how landform

surfaces change over time. Several moraines in this region have different ages, which allows for observations of how grain size distributions change over time. To characterize transport rates, experiments were conducted to observe individual grain transport as well as volumetric grain transport for varying grain sizes. These parameters were represented within a diffusion-based mathematical model as constants to predict grain size distributions along a hillslope. The diffusion-based model makes use of the hillslope diffusion equation, $dz/dt = \kappa(d^2z/dx^2)$, which calculates the change in hillslope elevation as a function of hillslope curvature. The change in elevation can be attributed to a change in volume of regolith that moves in and out of a certain point on the hillslope.

The first objective of this project was to acquire transport rate measurements for several different grain sizes to see what transport trends are observed between different grain sizes. Transport characteristics of grains smaller than 1 mm are poorly understood, and because these fine grains comprise such a large percentage of regolith in arid regions, it is important to understand their contribution to regolith transport. Knowing the differences in transport rates allows us to understand how different grains sizes are differentiated along the slope.

The second objective of this project was to create a model that can predict grain size distributions along desert hillslopes. A diffusion-based model was built to fulfill this objective, because hillslope diffusion has been used to accurately explain the general patterns of degradation seen in this region (Hallet and Putkonen, 1994). By inputting parameters into the model that generate the observed grain size distributions, and comparing those parameters to field measurements, their similarities and differences were examined to draw insights about how grains are differentiated on hillslopes.

The first main finding of this study is: transport rates do not necessarily increase with decreasing grains size. This claim is based on the field measurements of varying grain sizes, the grain size distributions observed in the field, laboratory tests, and mathematical modeling. Field experiments showed that annually, 0.7 mm diameter grains have a lower surface velocity than 3 mm grains at all slope angles, and that 30 mm pebbles traveled slowest out of the three grain sizes measured for surface. This was somewhat surprising, because past studies have indicated that typically, decreasing grain size will result in an increased transport rate. Attempts to replicate the field conditions within the laboratory showed that during rainfall events, neither the 0.7 mm nor 3 mm grains seemed to exhibit any movement unless a small mass wasting event was triggered, which caused similar transport distances between them. The 0.7 mm grains were much more susceptible to rapid burial, which would prevent them from being transported within the mobile layer of sediment if buried too deeply. The 3 mm grains do not become buried as easily, which might allow them to move more steadily down the slope, as opposed to intermittent transport of smaller grains as they are buried and uncovered.

On a dry surface, the 3 mm grains were more susceptible to moving downslope than the 0.7 mm grains. This indicates that mobilization events that occur in dry conditions (wind and animal activity) may play a larger role in differentiating grains than previously thought.

Sediment trap measurements showed that volumetric flux of grains at the surface are highest for grains 1.2 – 4.0 mm in diameter. The similarity between trends of surface velocities and surface flux of grains indicates that they are likely correlated for different grain sizes.

The second main finding of this study is: using a diffusion-based hillslope degradation model, it is possible to generate somewhat reliable predictions of how grain size distribution evolves on a hillslope over a given timeframe. The ability to predict grain size distributions as a function of both time and space is important for determining locations of slope stability as well as interpreting ages of landforms. A model that can accurately predict landform degradation and grain size distribution is a powerful tool that can both provide a practical purpose and supplement our scientific understanding of the way the Earth's surface changes through time.

APPENDIX

Field site coordinates

Site Name	Easting	Northing
AG-MBO-1-2017	-119.13641	37.87791
AG-MBY-2-2017	-119.12641	37.89954
AG-MBY-3-2017	-119.13115	37.89689
PB-MBO-1-2017	-119.13646	37.87791
PB-MBY-2-2017	-119.12646	37.8996
PB-MBY-3-2017	-119.13103	37.89689
SS-MBO-1-2017	-119.13019	37.88083
SS-MBO-2-2017	-119.12991	37.8801
SS-MBO-3-2017	-119.12939	37.87891
SS-MBY-1-2017	-119.13022	37.89766
SS-MBY-2-2017	-119.12984	37.89725
SS-MBY-3-2017	-119.13013	37.89677

NWS weather station data for Lee Vining, CA, from 5/17/2017 to 8/26/2017

Date	Max Temp (°C)	Min Temp (°C)	Rainfall (cm)
5/17/2017	12.2	1.1	0.00
5/18/2017	14.4	-1.1	0.00
5/19/2017	16.1	0.0	0.00
5/20/2017	21.1	2.8	0.00
5/21/2017	23.9	5.6	0.00
5/22/2017	23.9	6.1	0.00
5/23/2017	25.6	7.8	0.00
5/24/2017	20.0	8.3	0.00
5/25/2017	23.3	12.2	0.00
5/26/2017	22.2	2.8	0.00
5/27/2017	22.8	5.0	0.00
5/28/2017	22.8	5.0	0.00
5/29/2017	25.0	6.7	0.00
5/30/2017	26.1	8.3	0.00
5/31/2017	26.1	11.1	0.00
6/1/2017	15.6	4.4	0.00

6/2/2017	23.9	7.2	0.00
6/3/2017	27.2	10.0	0.00
6/4/2017	27.2	9.4	0.00
6/5/2017	25.0	6.7	0.00
6/6/2017	26.7	8.9	0.00
6/7/2017	28.3	7.8	0.00
6/8/2017	27.8	11.1	0.00
6/9/2017	18.9	10.6	0.00
6/10/2017	21.7	6.1	0.00
6/11/2017	21.1	6.7	0.00
6/12/2017	12.2	0.6	0.00
6/13/2017	14.4	0.0	0.00
6/14/2017	23.3	5.0	0.00
6/15/2017	26.7	7.8	0.00
6/16/2017	28.3	10.6	0.00
6/17/2017	30.0	12.8	0.00
6/18/2017	32.2	13.9	0.00
6/19/2017	30.6	13.9	0.13
6/20/2017	33.3	13.9	0.00
6/21/2017	33.9	14.4	0.00
6/22/2017	32.8	13.3	0.00
6/23/2017	31.7	13.9	0.00
6/24/2017	32.2	13.3	0.00
6/25/2017	31.7	12.8	0.00
6/26/2017	31.1	12.8	0.00
6/27/2017	27.8	8.3	0.00
6/28/2017	28.3	8.3	0.00
6/29/2017	27.8	8.3	0.00
6/30/2017	29.4	10.6	0.00
7/1/2017	31.1	11.7	0.00
7/2/2017	30.0	11.7	0.00
7/3/2017	31.1	12.8	0.00
7/4/2017	31.7	13.3	0.00
7/5/2017	31.1	12.2	0.00
7/6/2017	30.0	13.3	0.00
7/7/2017	31.1	13.3	0.00
7/8/2017	32.8	13.3	0.00
7/9/2017	32.8	15.6	0.00
7/10/2017	31.7	13.3	0.00
7/11/2017	30.0	13.3	0.00
7/12/2017	29.4	10.6	0.00

7/13/2017	31.1	13.9	0.00
7/14/2017	30.6	12.8	0.00
7/15/2017	31.7	13.9	0.00
7/16/2017	32.2	14.4	0.00
7/17/2017	30.6	12.8	0.00
7/18/2017	30.0	10.6	0.00
7/19/2017	28.3	10.0	0.00
7/20/2017	31.7	12.8	0.00
7/21/2017	31.1	14.4	0.00
7/22/2017	32.2	13.3	0.00
7/23/2017	32.8	14.4	0.00
7/24/2017	32.8	14.4	0.25
7/25/2017	29.4	13.3	0.00
7/26/2017	28.9	12.2	0.00
7/27/2017	28.9	12.2	0.00
7/28/2017	29.4	11.7	0.00
7/29/2017	31.1	12.2	0.00
7/30/2017	30.6	12.8	0.00
7/31/2017	31.1	13.3	0.00
8/1/2017	32.2	13.9	0.00
8/2/2017	32.8	15.6	0.00
8/3/2017	33.3	15.0	0.00
8/4/2017	32.2	16.7	0.00
8/5/2017	30.6	13.9	0.41
8/6/2017	26.7	10.0	0.28
8/7/2017	25.6	10.6	0.15
8/8/2017	27.8	11.7	0.00
8/9/2017	28.3	12.2	0.00
8/10/2017	27.2	10.6	0.30
8/11/2017	29.4	11.7	0.00
8/12/2017	29.4	11.7	0.00
8/13/2017	28.9	11.7	0.00
8/14/2017	29.4	11.7	0.00
8/15/2017	26.7	10.6	0.00
8/16/2017	26.7	12.2	0.00
8/17/2017	28.3	11.7	0.00
8/18/2017	28.9	12.8	0.00
8/19/2017	30.0	12.8	0.00
8/20/2017	28.9	11.1	0.00
8/21/2017	27.8	11.1	0.08
8/22/2017	26.1	11.7	0.00

8/23/2017	27.2	10.0	0.05
8/24/2017	27.2	11.7	0.00
8/25/2017	28.9	12.2	0.00
8/26/2017	29.4	12.8	0.00
Total			**1.65**

MATLAB code for hillslope diffusion model

```
%clear figures
clf
clear all

%Duration of simulation
maxtime = 100000; %Years (Tahoe: 45000; Mono Basin: 100000)

%------------------------
%Setup of initial slope profile. Current dimensions are for the Mono Basin
moraine.
xdistance=zeros(1,6000);
ydistance=zeros(1,6000);
yelevation=zeros(1,6000);

alfa=30;
counter=1;
for counter=1:1800; %(Change 1800 to 2100 for Tahoe moraine)
   xdistance(counter)=counter;
   ydistance(counter)=0;
   counter=counter+1;
end
for counter=1801:3000; %(Change 1801 to 2101 for Tahoe moraine)
   xdistance(counter)=counter;
   ydistance(counter)=ydistance(counter-1)+(xdistance(counter)-
xdistance(counter-1))*(tan((alfa/360)*2*3.1415927));
   counter=counter+1;
end
for counter=3001:6000;
   xdistance(counter)=counter;
   ydistance(counter)=ydistance(6001-counter);
   counter=counter+1;
end
for counter=4001:6000;
  xdistance(counter)=counter;
  ydistance(counter)=0;
  counter=counter+1;
end
slope_original = ydistance;
node_count=length(xdistance);
%------------------------------
```

```
%%%%%%%%%%%%%%%%%%%%%%%%%%%%%%%%%%%%%%%%%%%%%%%%%%%%%%%%%%%%%%%%%%%%%%%%%%%%
%Basic diffusion profile
%%%%%%%%%%%%%%%%%%%%%%%%%%%%%%%%%%%%%%%%%%%%%%%%%%%%%%%%%%%%%%%%%%%%%%%%%%%%
%This profile is generated so that the profile from the
%suface-based diffusion model can be compared to this one.

%Time increment
dt=0.5; %Years

%Horizontal increment
dx=0.1; %meters

%Kappa values
KXSmall = 0.002;
KSmall = 0.002;
KMedium = 0.002;
KMedLar = 0.002;
KLarge = 0.002;
KTotal = KXSmall+KSmall+KMedium+KMedLar+KLarge;%0.01 for Mono Basin moraine,
0.005 for Tahoe moraine

slope_height = slope_original;

%Starts loop on 2nd node
node_now=2;

for time_now=0:dt:maxtime

    for node_now=2:node_count-1

        %Diffusion equation
        slope_height(node_now)=slope_height(node_now)-(-
KTotal*(((slope_height(node_now-1)-...
        slope_height(node_now))/dx)-(slope_height(node_now)-
slope_height(node_now+1))/dx)*dt/dx);

        node_now = node_now + 1;

    end

end

%%%%%%%%%%%%%%%%%%%%%%%%%%%%%%%%%%%%%%%%%%%%%%%%%%%%%%%%%%%%%%%%%%%%%%%%%%%%
%Grain size distribution diffusion model
%%%%%%%%%%%%%%%%%%%%%%%%%%%%%%%%%%%%%%%%%%%%%%%%%%%%%%%%%%%%%%%%%%%%%%%%%%%%

%Time increment
dt=0.5; %Years

%Horizontal increment
dx=0.1; %meters
```

```
%Transport factor values
KXSmall = 0.0022;
KSmall = 0.0022;
KMedium = 0.0024;
KMedLar = 0.0022;
KLarge = 0.0009;
KTotal = KXSmall+KSmall+KMedium+KMedLar+KLarge;

%Active volume
active_volume = 1; %decimeters

%Q-values
qXSmall = zeros(1,3000);
qSmall = zeros(1,3000);
qMedium = zeros(1,3000);
qMedLar = zeros(1,3000);
qLarge = zeros(1,3000);

%Initial grain percents
initial_percent_xsmall = 0.10;
initial_percent_small = 0.10;
initial_percent_medium = 0.20;
initial_percent_medlar = 0.20;
initial_percent_large = 0.40;

%Initialize active percent of each grain size
active_percent_xsmall = ones(1,3000)*initial_percent_xsmall;
active_percent_small = ones(1,3000)*initial_percent_small;
active_percent_medium = ones(1,3000)*initial_percent_medium;
active_percent_medlar = ones(1,3000)*initial_percent_medlar;
active_percent_large = ones(1,3000)*initial_percent_large;

%Following variables monitor weight percent of grain sizes at certain
%places on the moraine
xsmall_footslope_array = 0;
small_footslope_array = 0;
medium_footslope_array = 0;
medlar_footslope_array = 0;
large_footslope_array = 0;

xsmall_midslope_array = 0;
small_midslope_array = 0;
medium_midslope_array = 0;
medlar_midslope_array = 0;
large_midslope_array = 0;

xsmall_crest_array = 0;
small_crest_array = 0;
medium_crest_array = 0;
medlar_crest_array = 0;
large_crest_array = 0;
```

```
time_array = [];

%Weathering rates for each grain size (%/half year, where 0.01 is 1%)
large_wr = 0.00001;
medlar_wr = 0
medium_wr = 0
small_wr = 0
xsmall_wr = 0;

%Imports raw profile to now use
slope_profile = slope_original;

for time=0:dt:maxtime

    %Shows time every 1000 years
    if rem(time, 1000) == 0
    time
    end

    %Calcluates hillslopes gradient for all segments of slope
    for i = 2:1:4000
        if slope_profile(i) - slope_profile(i-1) > 0.0000001
            dydx(i)=((slope_profile(i)/0.1) - (slope_profile(i-1)/0.1));
        end
    end

    %Calcluates slope angle in degrees for all points on slope
    slope_angle=abs(-atand(dydx/10));

    %Modifies initial % of grains through weathering
    initial_percent_large = initial_percent_large*(1-large_wr);
    initial_percent_medlar = initial_percent_medlar;
    initial_percent_medium = initial_percent_medium;
    initial_percent_small = initial_percent_small;
    initial_percent_xsmall = initial_percent_xsmall*(1+(large_wr));

    %These q values are the volume flux of each grain size in m^3/m-yr
    qXSmall = KXSmall*dydx*(dt/dx);
    qSmall = KSmall*dydx*(dt/dx);
    qMedium = KMedium*dydx*(dt/dx);
    qMedLar = KMedLar*dydx*(dt/dx);
    qLarge = KLarge*dydx*(dt/dx);
    qTotal = KTotal*dydx*(dt/dx);

    %Added_volume_x resets to zero each year along with lost_volume_x.
    %These will be used to find the yearly net volume of each grain size
    %by adding the latter to the former.

    added_volume_xsmall = zeros(1,3000);
    added_volume_small = zeros(1,3000);
    added_volume_medium = zeros(1,3000);
    added_volume_medlar = zeros(1,3000);
```

```
    added_volume_large = zeros(1,3000);

    lost_volume_xsmall = zeros(1,3000);
    lost_volume_small = zeros(1,3000);
    lost_volume_medium = zeros(1,3000);
    lost_volume_medlar = zeros(1,3000);
    lost_volume_large = zeros(1,3000);

    %Factors in surface availability to volume transported.
    for i = 5:1:3000
        if qTotal(i) > 0
        qzXSmall(i) = (qXSmall(i)*active_percent_xsmall(i));
        qzSmall(i) = (qSmall(i)*active_percent_small(i));
        qzMedium(i) = (qMedium(i)*active_percent_medium(i));
        qzMedLar(i) = (qMedLar(i)*active_percent_medlar(i));
        qzLarge(i) = (qLarge(i)*active_percent_large(i));
        qzTotal(i) = qzXSmall(i) + qzSmall(i) + qzMedium(i) + qzMedLar(i) +
qzLarge(i);

        qxXSmall(i) = (qzXSmall(i)/qzTotal(i))*qTotal(i);
        qxSmall(i) = (qzSmall(i)/qzTotal(i))*qTotal(i);
        qxMedium(i) = (qzMedium(i)/qzTotal(i))*qTotal(i);
        qxMedLar(i) = (qzMedLar(i)/qzTotal(i))*qTotal(i);
        qxLarge(i) = (qzLarge(i)/qzTotal(i))*qTotal(i);
        qxTotal(i) = qxXSmall(i) + qxSmall(i) + qxMedium(i) + qxMedLar(i) +
qxLarge(i);
        end
    end

        %All grain movement based on slope angles.
    for j=3000:-1:5;

        if slope_angle(j) >= 0

           added_volume_xsmall(j-1) = added_volume_xsmall(j-1) +
qxXSmall(j)*1.00;
           added_volume_xsmall(j-2) = added_volume_xsmall(j-2) +
qxXSmall(j)*0.00;
           added_volume_xsmall(j-3) = added_volume_xsmall(j-3) +
qxXSmall(j)*0.00;
           added_volume_xsmall(j-4) = added_volume_xsmall(j-4) +
qxXSmall(j)*0.00;
           lost_volume_xsmall(j) = -qxXSmall(j);

           added_volume_small(j-1) = added_volume_small(j-1) +
qxSmall(j)*1.00;
           added_volume_small(j-2) = added_volume_small(j-2) +
qxSmall(j)*0.00;
           added_volume_small(j-3) = added_volume_small(j-3) +
qxSmall(j)*0.00;
           lost_volume_small(j) = -qxSmall(j);
```

```
            added_volume_medium(j-1) = added_volume_medium(j-1) +
qxMedium(j)*1.00;
            added_volume_medium(j-2) = added_volume_medium(j-2) +
qxMedium(j)*0.00;
            added_volume_medium(j-3) = added_volume_medium(j-3) +
qxMedium(j)*0.00;
            added_volume_medium(j-4) = added_volume_medium(j-4) +
qxMedium(j)*0.00;
            lost_volume_medium(j) = -qxMedium(j);

            added_volume_medlar(j-1) = added_volume_medlar(j-1) +
qxMedLar(j)*1.00;
            added_volume_medlar(j-2) = added_volume_medlar(j-2) +
qxMedLar(j)*0.00;
            added_volume_medlar(j-3) = added_volume_medlar(j-3) +
qxMedLar(j)*0.00;
            lost_volume_medlar(j) = -qxMedLar(j);

            added_volume_large(j-1) = added_volume_large(j-1) +
qxLarge(j)*1.00;
            added_volume_large(j-2) = added_volume_large(j-2) +
qxLarge(j)*0.00;
            lost_volume_large(j) = -qxLarge(j);

        end

    end

    %Combine all added volumes and lost volumes at each node to get a
    %net volume for each node. The total net volume is the elevation that
    %the surface either lowers or raises.
    added_volume_total = added_volume_xsmall + added_volume_small +
added_volume_medium + added_volume_medlar + added_volume_large;
    lost_volume_total = lost_volume_xsmall + lost_volume_small +
lost_volume_medium + lost_volume_medlar + lost_volume_large;

    net_volume_xsmall = added_volume_xsmall + lost_volume_xsmall;
    net_volume_small = added_volume_small + lost_volume_small;
    net_volume_medium = added_volume_medium + lost_volume_medium;
    net_volume_medlar = added_volume_medlar + lost_volume_medlar;
    net_volume_large = added_volume_large + lost_volume_large;

    net_volume_total = net_volume_xsmall + net_volume_small +
net_volume_medium + net_volume_medlar + net_volume_large;

    %Add the net volume to the previous slope profile.
    slope_profile(1:3000) = slope_profile(1:3000) + net_volume_total(1:3000);

%-------------------------------------------------------------------------
    %Accumulation and erosion effects
    for i=5:1:3000
%-------------------------------------------------------------------------
        %Accumulation
```

```
        if net_volume_total(i) < active_volume && net_volume_total(i) > 0

            new_volume_xsmall(i) = ((active_volume -
net_volume_total(i))*active_percent_xsmall(i)) + net_volume_xsmall(i);
            new_volume_small(i) = ((active_volume -
net_volume_total(i))*active_percent_small(i)) + net_volume_small(i);
            new_volume_medium(i) = ((active_volume -
net_volume_total(i))*active_percent_medium(i)) + net_volume_medium(i);
            new_volume_medlar(i) = ((active_volume -
net_volume_total(i))*active_percent_medlar(i)) + net_volume_medlar(i);
            new_volume_large(i) = ((active_volume -
net_volume_total(i))*active_percent_large(i)) + net_volume_large(i);


%             %Omits volumes less than 0 (I don't think this ever happens but
%             %just in case)
%             if new_volume_xsmall(i) < 0
%             new_volume_xsmall(i) = 0;
%             end
%
%             if new_volume_small(i) < 0
%             new_volume_small(i) = 0;
%             end
%
%             if new_volume_medium(i) < 0
%                 new_volume_medium(i) = 0;
%             end
%
%             if new_volume_large(i) < 0
%                 new_volume_large(i) = 0;
%             end

            %New volume after factoring in net loss and gain
            new_volume_total(i) =
new_volume_xsmall(i)+new_volume_small(i)+new_volume_medium(i)+new_volume_medl
ar(i)+new_volume_large(i);

            active_percent_xsmall(i) =
new_volume_xsmall(i)/new_volume_total(i);
            active_percent_small(i) =
new_volume_small(i)/new_volume_total(i);
            active_percent_medium(i) =
new_volume_medium(i)/new_volume_total(i);
            active_percent_medlar(i) =
new_volume_medlar(i)/new_volume_total(i);
            active_percent_large(i) =
new_volume_large(i)/new_volume_total(i);

            %Weathering. Currently weathers large into xsmall
            new_w_volume_large(i) = new_volume_large(i)*(1-large_wr);
            new_w_volume_medlar(i) = (new_volume_medlar(i));
            new_w_volume_medium(i) = (new_volume_medium(i));
            new_w_volume_small(i) = (new_volume_small(i));
```

```
            new_w_volume_xsmall(i) = new_volume_xsmall(i) +
(large_wr*new_volume_large(i));

            new_w_volume_total(i) = new_w_volume_xsmall(i) +
new_w_volume_small(i) + new_w_volume_medium(i) + new_w_volume_medlar(i) +
new_w_volume_large(i);

            %Calculates available volume of each grain size at the surface.
            active_percent_xsmall(i) =
new_w_volume_xsmall(i)/new_w_volume_total(i);
            active_percent_small(i) =
new_w_volume_small(i)/new_w_volume_total(i);
            active_percent_medium(i) =
new_w_volume_medium(i)/new_w_volume_total(i);
            active_percent_medlar(i) =
new_w_volume_medlar(i)/new_w_volume_total(i);
            active_percent_large(i) =
new_w_volume_large(i)/new_w_volume_total(i);

        end

%-----------------------------------------------------------------
% %         %Erosion
        if net_volume_total(i) < 0

            new_volume_xsmall(i) = (active_volume*active_percent_xsmall(i)) +
net_volume_xsmall(i) - (net_volume_total(i)*initial_percent_xsmall);
            new_volume_small(i) = (active_volume*active_percent_small(i)) +
net_volume_small(i) - (net_volume_total(i)*initial_percent_small);
            new_volume_medium(i) = (active_volume*active_percent_medium(i)) +
net_volume_medium(i) - (net_volume_total(i)*initial_percent_medium);
            new_volume_medlar(i) = (active_volume*active_percent_medlar(i)) +
net_volume_medlar(i) - (net_volume_total(i)*initial_percent_medlar);
            new_volume_large(i) = (active_volume*active_percent_large(i)) +
net_volume_large(i) - (net_volume_total(i)*initial_percent_large);

            %Omits volumes less than 0 (I don't think this ever happens but
            %just in case (causes NaN)
            if new_volume_xsmall(i) < 0
            new_volume_xsmall(i) = 0;
            end

            if new_volume_small(i) < 0
            new_volume_small(i) = 0;
            end

            if new_volume_medium(i) < 0
                new_volume_medium(i) = 0;
            end

            if new_volume_medlar(i) < 0
            new_volume_medlar(i) = 0;
            end
```

```
            if new_volume_large(i) < 0
                new_volume_large(i) = 0;
            end

            new_volume_total(i) = new_volume_xsmall(i) + new_volume_small(i)
+ new_volume_medium(i) +new_volume_medlar(i) + new_volume_large(i);

            %Weathering. Currently weathers large into xsmall
            new_w_volume_large(i) = new_volume_large(i)*(1-large_wr);
            new_w_volume_medlar(i) = (new_volume_medlar(i));
            new_w_volume_medium(i) = (new_volume_medium(i));
            new_w_volume_small(i) = (new_volume_small(i));
            new_w_volume_xsmall(i) = new_volume_xsmall(i) +
(large_wr*new_volume_large(i));

            new_w_volume_total(i) = new_w_volume_xsmall(i) +
new_w_volume_small(i) + new_w_volume_medium(i) + new_w_volume_medlar(i) +
new_w_volume_large(i);

            %Calculates available volume of each grain size at the surface.
            active_percent_xsmall(i) =
new_w_volume_xsmall(i)/new_w_volume_total(i);
            active_percent_small(i) =
new_w_volume_small(i)/new_w_volume_total(i);
            active_percent_medium(i) =
new_w_volume_medium(i)/new_w_volume_total(i);
            active_percent_medlar(i) =
new_w_volume_medlar(i)/new_w_volume_total(i);
            active_percent_large(i) =
new_w_volume_large(i)/new_w_volume_total(i);

        end
 %--------------------------------------------------------------------

    end

    if rem(time,10) == 0

    %Following lines generate values for the weight % of each grain size at
    %certain places on the slope. To be plotted against time later on.
    xsmall_footslope = active_percent_xsmall(1400)*100;
    small_footslope = active_percent_small(1400)*100;
    medium_footslope = active_percent_medium(1400)*100;
    medlar_footslope = active_percent_medlar(1400)*100;
    large_footslope = active_percent_large(1400)*100;

    xsmall_footslope_array = [xsmall_footslope_array, xsmall_footslope];
    small_footslope_array = [small_footslope_array, small_footslope];
    medium_footslope_array = [medium_footslope_array, medium_footslope];
    medlar_footslope_array = [medlar_footslope_array, medlar_footslope];
    large_footslope_array = [large_footslope_array, large_footslope];
```

```
    xsmall_midslope = active_percent_xsmall(2250)*100;
    small_midslope = active_percent_small(2250)*100;
    medium_midslope = active_percent_medium(2250)*100;
    medlar_midslope = active_percent_medlar(2250)*100;
    large_midslope = active_percent_large(2250)*100;

    xsmall_midslope_array = [xsmall_midslope_array, xsmall_midslope];
    small_midslope_array = [small_midslope_array, small_midslope];
    medium_midslope_array = [medium_midslope_array, medium_midslope];
    medlar_midslope_array = [medlar_midslope_array, medlar_midslope];
    large_midslope_array = [large_midslope_array, large_midslope];

    xsmall_crest = active_percent_xsmall(3000)*100;
    small_crest = active_percent_small(3000)*100;
    medium_crest = active_percent_medium(3000)*100;
    medlar_crest = active_percent_medlar(3000)*100;
    large_crest = active_percent_large(3000)*100;

    xsmall_crest_array = [xsmall_crest_array, xsmall_crest];
    small_crest_array = [small_crest_array, small_crest];
    medium_crest_array = [medium_crest_array, medium_crest];
    medlar_crest_array = [medlar_crest_array, medlar_crest];
    large_crest_array = [large_crest_array, large_crest];

    time_array = [time_array, time];

    end

end

%%%%%%%%%%%%%%%%%%%%%%%%%%%%%%%%%%%%%%%%%%%%%%%%%%%%%%%%%%%%%%%%%%%%%%%%%%%%%%%
%End of diffusion model
%%%%%%%%%%%%%%%%%%%%%%%%%%%%%%%%%%%%%%%%%%%%%%%%%%%%%%%%%%%%%%%%%%%%%%%%%%%%%%%

%Convert active percent to out of 100 for aesthetics
active_percent_xsmall = active_percent_xsmall.*100;
active_percent_small = active_percent_small.*100;
active_percent_medium = active_percent_medium.*100;
active_percent_medlar = active_percent_medlar.*100;
active_percent_large = active_percent_large.*100;

%Calclates least squares for Tahoe moraine
if maxtime == 45000

    LS_XSmall_Young_Foot = (28-active_percent_xsmall(1800))^2;
    LS_XSmall_Young_Mid = (27-active_percent_xsmall(2400))^2;
    LS_XSmall_Young_Crest = (35-active_percent_xsmall(2950))^2;
    LS_XSmall_Young_Total =
LS_XSmall_Young_Foot+LS_XSmall_Young_Mid+LS_XSmall_Young_Crest;

    LS_Small_Young_Foot = (14-active_percent_small(1800))^2;
```

```
    LS_Small_Young_Mid = (11-active_percent_small(2400))^2;
    LS_Small_Young_Crest = (4-active_percent_small(2950))^2;
    LS_Small_Young_Total =
LS_Small_Young_Foot+LS_Small_Young_Mid+LS_Small_Young_Crest;

    LS_Medium_Young_Foot = (34-active_percent_medium(1800))^2;
    LS_Medium_Young_Mid = (26-active_percent_medium(2400))^2;
    LS_Medium_Young_Crest = (6-active_percent_medium(2950))^2;
    LS_Medium_Young_Total =
LS_Medium_Young_Foot+LS_Medium_Young_Mid+LS_Medium_Young_Crest;

    LS_MedLar_Young_Foot = (23-active_percent_medlar(1800))^2;
    LS_MedLar_Young_Mid = (20-active_percent_medlar(2400))^2;
    LS_MedLar_Young_Crest = (2-active_percent_medlar(2950))^2;
    LS_MedLar_Young_Total =
LS_MedLar_Young_Foot+LS_MedLar_Young_Mid+LS_MedLar_Young_Crest;

    LS_Large_Young_Foot = (1-active_percent_large(1800))^2;
    LS_Large_Young_Mid = (16-active_percent_large(2400))^2;
    LS_Large_Young_Crest = (53-active_percent_large(2950))^2;
    LS_Large_Young_Total =
LS_Large_Young_Foot+LS_Large_Young_Mid+LS_Large_Young_Crest;

    LS_Total = LS_XSmall_Young_Total + LS_Small_Young_Total +
LS_Medium_Young_Total + LS_MedLar_Young_Total + LS_Large_Young_Total

end

%Calculates least squares for Mono Basin moraine
if maxtime == 100000

    LS_XSmall_Old_Foot = (43-active_percent_xsmall(1000))^2;
    LS_XSmall_Old_Mid = (36-active_percent_xsmall(2100))^2;
    LS_XSmall_Old_Crest = (39-active_percent_xsmall(2950))^2;
    LS_XSmall_Old_Total =
LS_XSmall_Old_Foot+LS_XSmall_Old_Mid+LS_XSmall_Old_Crest;

    LS_Small_Old_Foot = (17-active_percent_small(1000))^2;
    LS_Small_Old_Mid = (14-active_percent_small(2100))^2;
    LS_Small_Old_Crest = (12-active_percent_small(2950))^2;
    LS_Small_Old_Total =
LS_Small_Old_Foot+LS_Small_Old_Mid+LS_Small_Old_Crest;

    LS_Medium_Old_Foot = (21-active_percent_medium(1000))^2;
    LS_Medium_Old_Mid = (25-active_percent_medium(2100))^2;
    LS_Medium_Old_Crest = (21-active_percent_medium(2950))^2;
    LS_Medium_Old_Total =
LS_Medium_Old_Foot+LS_Medium_Old_Mid+LS_Medium_Old_Crest;

    LS_MedLar_Old_Foot = (15-active_percent_medlar(1000))^2;
    LS_MedLar_Old_Mid = (21-active_percent_medlar(2100))^2;
    LS_MedLar_Old_Crest = (26-active_percent_medlar(2950))^2;
```

```
    LS_MedLar_Old_Total =
LS_MedLar_Old_Foot+LS_MedLar_Old_Mid+LS_MedLar_Old_Crest;

    LS_Large_Old_Foot = (4-active_percent_large(1000))^2;
    LS_Large_Old_Mid = (5-active_percent_large(2100))^2;
    LS_Large_Old_Crest = (2-active_percent_large(2950))^2;
    LS_Large_Old_Total =
LS_Large_Old_Foot+LS_Large_Old_Mid+LS_Large_Old_Crest;

    LS_Total = LS_XSmall_Old_Total + LS_Small_Old_Total + LS_Medium_Old_Total
+ LS_MedLar_Old_Total + LS_Large_Old_Total;

end

%Plot regular diffusion profile and new modeled slope profile atop one
%another
figure(1)
hold on
axis equal
plot(slope_original(1,1:3000));
plot(slope_height(1,1:3000));
plot(slope_profile(1,1:3000));
title('Slope profile')
xlabel('Horizontal Distance (dm)')
ylabel('Height (dm)')
hold off

%Allows profile to fit in distribution chart
slope_profile = (slope_profile/10);

%Plot grain size distributions for each grain size to be plotted against
%distance along hillslope
figure(2)
title('Mono Basin moraine (100,000 years)', 'FontSize', 12)
hold on
plot(active_percent_xsmall, 'g')
plot(active_percent_small, 'b')
plot(active_percent_medium, 'r')
plot(active_percent_medlar, 'c')
plot(active_percent_large, 'k')
plot(slope_profile(1,1:3000), 'LineStyle', '--', 'Color', [0.75 0.75 0.75]);
xlabel('Horizontal Distance (dm)', 'FontSize', 14)
ylabel('Weight %', 'FontSize', 14)
legend({'<0.58 mm', '0.58-1 mm', '1-4 mm', '4-27 mm', '27+ mm', 'slope
profile'}, 'Location', 'northwest', 'FontSize', 11)
xlim([1485 3000])
ylim([-3 100])

if maxtime == 100000
%-------------------------------------

   %Plot observed distributions at crest
   %27+mm
```

```
    plot(3000,2, 'ok', 'HandleVisibility', 'off');
    %3-27mm
    plot(3000,26, 'oc', 'HandleVisibility', 'off');
    %3mm
    plot(3000,21, 'or', 'HandleVisibility', 'off');
    %0.7mm
    plot(3000,12, 'ob', 'HandleVisibility', 'off');
    %<0.7mm
    plot(3000,39, 'og', 'HandleVisibility', 'off');

       %Plot observed distributions at midslope
    %27+ mm
    plot(2250,5, 'ok', 'HandleVisibility', 'off');
    %3-27mm
    plot(2250,21, 'oc', 'HandleVisibility', 'off');
    %3mm
    plot(2250,25, 'or', 'HandleVisibility', 'off');
    %0.7mm
    plot(2250,14, 'ob', 'HandleVisibility', 'off');
    %<0.7mm
    plot(2250,36, 'og', 'HandleVisibility', 'off');

       %Plot observed distributions at footslope
    %27+ mm
    plot(1500,4, 'ok', 'HandleVisibility', 'off');
    %3-27mm
    plot(1500,15, 'oc', 'HandleVisibility', 'off');
    %3mm
    plot(1500,21, 'or', 'HandleVisibility', 'off');
    %0.58-1mm
    plot(1500,17, 'ob', 'HandleVisibility', 'off');
    %<0.58mm
    plot(1500,43, 'og', 'HandleVisibility', 'off');

end

if maxtime == 45000

    %Plot observed distributions at crest
    %27+ mm
    plot(3000,53, 'ok', 'HandleVisibility', 'off');
    %4-27mm
    plot(3000,2, 'oc', 'HandleVisibility', 'off');
    %1-4mm
    plot(3000,6, 'or', 'HandleVisibility', 'off');
    %0.58-1mm
    plot(3000,4, 'ob', 'HandleVisibility', 'off');
    %<0.58mm
    plot(3000,35, 'og', 'HandleVisibility', 'off')

       %Plot observed distributions at midslope
    %27+ mm
    plot(2400,16, 'ok', 'HandleVisibility', 'off');
```

```
    %4-27mm
    plot(2400,20, 'oc', 'HandleVisibility', 'off');
    %1-4mm
    plot(2400,26, 'or', 'HandleVisibility', 'off');
    %0.7mmadde
    plot(2400,11, 'ob', 'HandleVisibility', 'off');
    %<0.7mm
    plot(2400,27, 'og', 'HandleVisibility', 'off');

       %Plot observed distributions at footslope
    %27+ mm
    plot(1800,1, 'ok', 'HandleVisibility', 'off');
    %4-27mm
    plot(1800,23, 'oc', 'HandleVisibility', 'off');
    %1-4mm
    plot(1800,34, 'or', 'HandleVisibility', 'off');
    %0.58-1mm
    plot(1800,14, 'ob', 'HandleVisibility', 'off');
    %<0.58mm
    plot(1800,28, 'og', 'HandleVisibility', 'off');

end

x = [4500 4500];
y = [2 60];

x1 = [9990 9990];
y1 = [2 60];

%Figures for grain size distribution vs. time
figure(3)
title('Time vs. grain size distribution (footslope)', 'FontSize', 12)
hold on
plot(xsmall_footslope_array, 'g');
plot(small_footslope_array, 'b');
plot(medium_footslope_array, 'r');
plot(medlar_footslope_array, 'c');
plot(large_footslope_array, 'k');
plot(x,y, 'LineStyle', '--', 'Color', [0.75 0.75 0.75]);
plot(x1,y1, 'LineStyle', '--', 'Color', [0.75 0.75 0.75]);
xticks([10 2000 4000 6000 8000 10000]);
xticklabels({'0','20','40','60','80','100'});
xlabel('Time (kyr)', 'FontSize', 14);
ylabel('Weight %', 'FontSize', 14);
legend({'<0.58 mm', '0.58-1 mm', '1-4 mm', '4-27 mm', '27+ mm'}, 'Location',
'northwest', 'FontSize', 11);
xlim([1 10000])
ylim([-3 100])

figure(4)
title('Time vs. grain size distribution (crest)', 'FontSize', 12)
hold on
plot(xsmall_crest_array, 'g');
```

```
plot(small_crest_array, 'b');
plot(medium_crest_array, 'r');
plot(medlar_crest_array, 'c');
plot(large_crest_array, 'k');
plot(x,y, 'LineStyle', '--', 'Color', [0.75 0.75 0.75]);
plot(x1,y1, 'LineStyle', '--', 'Color', [0.75 0.75 0.75]);
xticks([10 2000 4000 6000 8000 10000]);
xticklabels({'0','20','40','60','80','100'});
xlabel('Time (kyr)', 'FontSize', 14);
ylabel('Weight %', 'FontSize', 14);
legend({'<0.58 mm', '0.58-1 mm', '1-4 mm', '4-27 mm', '27+ mm'}, 'Location',
'northwest', 'FontSize', 11);
xlim([1 10000])
ylim([-3 100])
```

REFERENCES

Abrahams, A., Parsons, A., Cooke, R., Reeves, R., 1984, Stone movement on hillslopes in the Mojave Desert, California: A 16-year record. Earth Surface Processes and Landforms. Vol. 9, p. 365-370.

Carson, M.A. and Kirkby, M.J., 1972, Hillslope form and Process. Earth Science Reviews, Vol. 8, Iss. 3, p. 343-344.

Culling, W.E.H., 1960, Analytical theory of erosion. Journal of Geology, vol. 68, p. 336-344.

Darwin, C., 1881, The Formation of Vegetable Mould, through the Actions of Worms, with Observations on Their Habits, John Murray, London, UK.

Davis,W.M. 1892, The convex profile of bad-land divides. Science Vol. 20, p. 245

Freeman, R. B., 1977, The Works of Charles Darwin: An Annotated Bibliographical Handlist. Folkestone. Wm Dawson & Sons Ltd. Retrieved 4 November 2008. Print.

Gabet, E., 2003, Sediment transport by dry ravel, Journal of Geophysical Research, v. 108, p. 22-4.

Gillespie, A.R., and Clark, D., 2011, Glaciations of the Sierra Nevada, California, USA, Developments in Quaternary Science. Vol. 15, p. 447-462.

Hallet, B., Putkonen, J.,1994, Surface Dating of Dynamic Landforms: Young Boulders on Aging Moraines. Science, Vol. 265, p. 937-940.

Kirkby, A., and Kirkby, M.J., 1974, Surface wash at the semi-arid break in slope. Zeitschrift fur Geomorphologie N.F., Vol. 21, no. 2, p. 151-176.

Kirkby, M., Statham, I., 1975, Surface stone movement and scree formation. The Journal of Geology, Vol. 83(3), p. 349-362.

Leopold, L. B., Emmett, W. W., Myrick, R. M., 1966, Channel and hillslope processes in a semiarid area, New Mexico. US Geological Survey Professional Paper 352-G, p. 193-252.

Madoff, R., 2015, Climate drive hillslope degradation of Mono Basin moraine, Eastern Sierra Nevada, USA. Doctoral dissertation.

Melton, M., 1965, Debris-covered hillslopes of the southern Arizona desert: consideration of their stability and sediment contribution. The Journal of Geology, Vol. 73(5), p. 715-729.

McLaren, P., Bowles, D, 1985, The effects of sediment transport on grain size distributions. Journal of Sedimentary Petrology, Vol. 55, No. 4, p. 457-470.

National Research Council, 2000, Guidelines for determining flood hazards on alluvial fans, report, 23 pp., Fed. Emergency Manage Agency, Washington, D. C., 23 Feb.

Phillips, F., Zreda, M., Smith, S., Elmore, D., Kubik, P., Sharma, P., 1990, Cosmogenic Chlorine-36 Chronology for Glacial Deposits at Bloody Canyon, Eastern Sierra Nevada. Science, Vol. 248, Iss. 4926.

Putkonen, J. and O'Neal, M., 2006. Degradation of unconsolidated Quaternary landforms in the western North America. Geomorphology, Vol. 75, p. 408– 419.

Putkonen, J., and Swanson, T., 2003. Accuracy of cosmogenic ages for moraines. Quaternary Research, Vol. 59, p. 255–261.

Putkonen, J., Morgan, D., Balco, G., 2012. Regolith transport quantified by braking block, McMurdo Dry Valleys, Antarctica. Geomorphology vol. 155–156, p. 80–87.

Sampson, K., Smith, L., 2006, Relative ages of Pleistocene moraines discerned from pebble counts: eastern Sierra Nevada, California. Physical Geography, 27, 7, p. 223-235.

Saunders, I. and Young, A., 1983, Rates of surface processes on slopes, slope retreat and denudation. Earth Surface Processes and Landforms, vol. 8, p. 473-501.

Schumm, S.A., 1967, Rates of Surficial Rock Creep on Hillslopes in Western Colorado. Science, p. 223, 230.

Scheidegger, A. E., 1961, Mathematical models of slope development. Geological Society of America Bulletin, Vol. 72, p. 37-50.

Selby, M.J., 1982, Hillslope materials and processes, Oxford University Press, p. 208.

Shi, Z.H., Fang, N.F., Wu, F.Z., Wang, L., Yue, B.J., Wue, G.L, 2012, Soil erosion processes and sediment sorting associated with transport mechanisms on steep slopes. Journal of Hydrology v. 454–455 p. 123–130.

Statham, I., 1973, Scree slope development under conditions of surface particle movement. Transactions of the Institute of British Geographers, No. 59, p. 41-53.

Statham, I., 1977, Earth surface sediment transport, Clarendon Press, p. 35.

Van Burkalow, A., 1945, Angle of repose and angle of sliding friction: an experimental study. Bulletin of the Geological Society of America, Vol. 56, p. 669-708.

Visher, G., 1969, Grain size distributions and depositional processes. Journal of Sedimentary Petrology, Vol. 39(3), p. 1074-1106.

Waters, M., 1997, Principles of Geoarchaeology: A North American Perspective. University of Arizona Press, Chapter 2.

Wells, W.G. II; Wohlgemuth, P.M., 1987, Sediment traps for measuring onslope surface sediment movement. Res. Note PSW-RN-393. Berkeley, CA: Pacific Southwest Research Station, Forest Service, U.S. Department of Agriculture; 6 p.

Zhou, J., Shi, C., Fu-gang, X., 2013, Geotechnical characteristics and stability analysis of rock-soil aggregate slope at the Gushui Hydropower Station, Southwest China. Scientific World Journal, Vol. 2013